Characteristics of Thermal Finestructure in the Southern Yellow Sea and the East China Sea from Airborne Expendable Bathythermograph Measurements

Sunghyea Park and Peter C. Chu
Department of Oceanography, Naval Postgraduate School, Monterey, California

Corresponding author's address
Sunghyea Park
Department of Oceanography, Naval Postgraduate School,
Monterey, CA93943-5001, USA
Tel: 1-831-656-7819 Fax: 1-831-656-3686
Email: spark@nps.edu

Key words: Yellow/East China Seas, AXBT, synoptic thermal fronts, thermal finestructures, mixing

Report Documentation Page

Form Approved
OMB No. 0704-0188

Public reporting burden for the collection of information is estimated to average 1 hour per response, including the time for reviewing instructions, searching existing data sources, gathering and maintaining the data needed, and completing and reviewing the collection of information. Send comments regarding this burden estimate or any other aspect of this collection of information, including suggestions for reducing this burden, to Washington Headquarters Services, Directorate for Information Operations and Reports, 1215 Jefferson Davis Highway, Suite 1204, Arlington VA 22202-4302. Respondents should be aware that notwithstanding any other provision of law, no person shall be subject to a penalty for failing to comply with a collection of information if it does not display a currently valid OMB control number.

1. REPORT DATE	2. REPORT TYPE	3. DATES COVERED
2008		**00-00-2008 to 00-00-2008**

4. TITLE AND SUBTITLE	5a. CONTRACT NUMBER
Characteristics of Thermal Finestructure in the Southern Yellow Sea and the East China Sea from Airborne Expendable Bathythermograph Measurements	5b. GRANT NUMBER
	5c. PROGRAM ELEMENT NUMBER
6. AUTHOR(S)	5d. PROJECT NUMBER
	5e. TASK NUMBER
	5f. WORK UNIT NUMBER
7. PERFORMING ORGANIZATION NAME(S) AND ADDRESS(ES) **Department of Oceanography,Naval Postgraduate School,Monterey ,CA,93943**	8. PERFORMING ORGANIZATION REPORT NUMBER
9. SPONSORING/MONITORING AGENCY NAME(S) AND ADDRESS(ES)	10. SPONSOR/MONITOR'S ACRONYM(S)
	11. SPONSOR/MONITOR'S REPORT NUMBER(S)

12. DISTRIBUTION/AVAILABILITY STATEMENT
Approved for public release; distribution unlimited

13. SUPPLEMENTARY NOTES

14. ABSTRACT

15. SUBJECT TERMS

16. SECURITY CLASSIFICATION OF:			17. LIMITATION OF ABSTRACT	18. NUMBER OF PAGES	19a. NAME OF RESPONSIBLE PERSON
a. REPORT **unclassified**	b. ABSTRACT **unclassified**	c. THIS PAGE **unclassified**	**Same as Report (SAR)**	**59**	

Abstract

Four surveys of airborne expendable bathythermograph with horizontal spacing of about 35 km and vertical spacing of 1 m extending from the surface down to 400 m deep are used to analyze thermal finestructures and their seasonality in frontal zones of the southern Yellow Sea and the East China Sea. Finestructure characteristics are different not only among fronts but also along the same front, implying different mixing mechanisms. Summer thermocline intrusions with thickness from few to 40 meters generated by the vertically-sheared advection, are identified along the southern tongue of the Cheju–Yangtze Front (especially south of Cheju Island). The finestructures south of the Yangtze Bank (i.e., the western tip of the southern tongue) produced by strong along-frontal currents are not as rich as elsewhere in the southern tongue. The Cheju–Tsushima Front presents mixed finestructures due to confluent currents from various origins. The irregular-staircase finestructures in the Kuroshio region (below the seasonal thermocline) driven by double-diffusive mixing show seasonal invariance and vertical/horizontal coherence. The strength of mixing related to finestructure is weaker in the Kuroshio region than in the Cheju–Tsushima Front or south of Cheju Island. The profiles in the Tsushima Warm Current branching area show large (~50 m thick) irregular-staircase structures at upper 230 m depth, which coincides roughly with the lower boundary of maximum salinity layer. The finestructure at deeper 230 m depth is similar to that in the Kuroshio region. The possible mechanisms for generating the finestructures are also discussed.

1. Introduction

Temperature and salinity profiles are smooth curves (or straight lines) or ragged curves (i.e. a variety of vertical variations). The vertical variation with scales of 1–100 m is termed as 'finestructure' and that with scales smaller than 1 m is termed as 'microstructure' (Warren and Wunsch, 1981). The finestructure is observed in various forms, and some of them, which are frequently observed and detected, are named as follows: (1) staircase, also called steppy or stepwise structure (Schmitt *et al.*, 1987; Zodiatis and Gasparini, 1996), when temperature and salinity profiles show alternative sheets [strong temperature/salinity gradient in short vertical distance such as d_1 to d_2 (~1 m) or d_3 to d_4 (~ 2 m) in Fig. 1a] and layers [almost isothermal/isohaline or low gradient in rather longer vertical distance such as d_2 to d_3 (~13 m) in Fig. 1a]; (2) thermocline/halocline intrusion, when temperature and salinity profiles display multilayered structures at the thermocline/halocline depths [Ruddick and Richards, 2003; see intrusive structures at 50–100 m (50–90 m) depth in profile 2 (3) in Fig. 1b]; and (3) interleaving, which is similar to the thermocline/halocline intrusion and is highlighted by large, even O (100 km) in the equatorial Pacific, horizontal continuity of multilayered structures (Richards and Banks, 2002; Lee and Richards, 2004). In addition, there are mixed, eroded versions of these forms, and any forms are also possible (Fig. 1c). These finestructures are common anywhere in oceans but more complex and heterogeneous around fronts and current confluence zones (Joyce, 1976; Williams, 1981; Bianchi *et al.*, 1993).

Numerous analyses on finestructures have been conducted in the tropics (Mcphaden, 1985; Richards and Banks, 2002; Lee and Richards, 2004), the Antarctic (Georgi, 1978, 1981; Toole, 1981), the Atlantic (Joyce, 1976; Schmitt and Georgi, 1982; Schmitt *et al.*, 1986), and the Pacific (Gregg, 1977; Peters *et al.*, 1991). A new seismic reflection methodology produces snapshots of finestructures at high lateral sampling (< 10 m) in the Norwegian Sea (Nandi *et al.*, 2004). These analyses enhance the knowledge of mixing processes of water mass, energy transformation, and internal wave kinematics. However, finestructures or mixing processes in the Yellow Sea and the East China Sea (YES) have been less studied, although the YES exhibits various thermohaline finestructures induced by the Kuroshio intrusion, enormous river discharge, strong tidal currents, and internal waves in the well-developed shelves along with trenches (Chu et al., 1997a, b; 2005).

Bao *et al.* (1996) analyzed the vertical scales and spectral characteristics of the finestructures southwest off Kyushu using springtime profiles and addressed the finestructure characteristics with respect to water mass distributions. Lee *et al.* (2003) reported cross-frontal thermal intrusion with 5–10 m thickness southeast off Cheju Island and several high or low salinity cores with horizontal scales of tens kilometers southwest of the Tsushima Warm Current branching region. In addition, several studies showed thermohaline finestructures (Lie *et al.*, 1998; Lie *et al.*, 2000; Lie *et al.*, 2003) but did not provide detail information. Park and Chu (2006) suggested that the frontal mixing in both temperature and salinity fields is vigorous in the region connecting to the Yangtze Bank,

the Cheju Strait, and the Korea Strait. Their suggestion is based on the analysis of the surface and subsurface thermal and haline fronts throughout YES from a climatological dataset [i.e., Generalized Digital Environmental Model (GDEM)] in terms of frontal intensity, water mass distribution, and temporal evolutions of temperature and salinity across the fronts. However, finestructure and its seasonality were not investigated due to the limitation of the climatological data.

Recently, new thermal features were discovered using four airborne expendable bathythermograph (AXBT) surveys with horizontal spacing of 35 km and vertical resolution of 1 m from the surface to 400 m depth over the southern Yellow Sea (YS) and the East China Sea (ECS) in September 1992 and February, May, and September 1993 (Furey and Bower, 2005; Park and Chu, 2007a, b). Furey and Bower (2005) analyzed variability of mixed layer depth, path change of the Kuroshio associated with the generation of cold eddies on canyons northeast off Taiwan, and seasonal evolution of thermal fronts in YES and the Japan/East Sea. Park and Chu (2007a) identified synoptic distributions of thermocline and thermal surface mixed layer [with different definition compared to Furey and Bower (2005)], as well as seasonality and dominate driving mechanism of the surface mixed layer. Park and Chu (2007b) further investigated the synoptic features in/around thermal fronts and the cross-frontal heat fluxes that have not been described in detail previously. The thermal finestructures in/around the fronts, such as the thermocline intrusions, ragged isotherms, and multilayered temperature inversions, were described by Park and Chu (2007b) qualitatively but not quantitatively.

Since the fronts in the YES are linked dynamically to the current system comprising the Kuroshio, the Taiwan Warm Current, the Tsushima Warm Current, and the Cheju Warm Current, these AXBT data with sufficiently large horizontal coverage are useful to examine the finestructures across a front or among different fronts regarding surrounding conditions such as frontal features, water masses, and the current system. They are also invaluable to identify the seasonal variability of the finestructures in the YES.

The goal of this study is to analyze characteristics of thermal finestructures, including their seasonality, by frontal zones in the YES using the AXBT data. For the lack of concurrent salinity/velocity data and time-series data for analysis, it is difficult to elucidate generation mechanisms of the finestructure with concrete evidences. Instead, using the AXBT data, CTD data (observed at different time) and hydrographic plots in other studies, we propose plausible generation mechanisms of the finestructures and related mixing processes in connection to the surrounding thermal features, water masses, and circulation systems.

The rest of the paper is organized as follows. Section 2 introduces the AXBT data. Section 3 describes finestructures in the profiles grouped by the frontal zones. Section 4 analyzes ensemble-averaged spectra and statistical characteristics of groups with rich finestructures. Section 5 examines finestructures of each profile in the region where the Tsushima Warm Current is originated from the Kuroshio. Section 6 presents conclusions.

2. Data

The AXBT data, a part of the Master Oceanographic Observation Data Set (MOODS) maintained by the Naval Oceanographic Office (NAVOCEANO), Stennis Space Center, Mississippi, were obtained under the approval by NAVOCEANO. The AXBT data including their detail information have not been open to the public yet. Accordingly, few references have been available although the AXBT data were collected in the early 1990s. In 1990s, Sparton AXBTs were widely used in U.S. Navy research. Their thermal time constant 0.1 s or less and their vertical resolution is 15 cm (Boyd and Linzell, 1993). We obtained the edited AXBT data with 1 meter vertical resolution. The editing process includes indentifying recording errors and outliers, checking duplicate profiles, checking depth inversion and depth duplication for individual profiles, checking temperature range, checking large temperature inversions and gradients, checking standard deviation, interpolation to standard levels, and post objective analysis checks (Teague, 1986; Jugan and Beresford, 1992; Boyer and Levitus, 1994; Chu et al., 1997c, 1998). The accuracy of the data depends on the accuracy of conversion equations, which transform frequency into temperature and elapsed fall time into depth: the AXBT does not measure depth directly. Customized equations, which were achieved using concurrent CTD data, provide the accuracy of temperature data of 0.13^{o}C and that of depth of ±2% of depth or ±10 m, whichever is greater. The Naval Research Laboratory (NRL) Isis System determines the AXBT frequency to such accuracy that the resulting temperature accuracy is 0.05^{o}C or better (Boyd and Linzell, 1993).

The AXBT data used in this study consist of 1256 profiles from the four surveys (Fig. 2a): 18−29 September 1992 (named as 9209), 4−14 February 1993 (as 9302), 5−14 May 1993 (as 9305), and 2−10 September 1993 (as 9309). The four surveys almost repeated themselves in track paths with slight mismatches and were completed within one week except for some profiles near the Korea/Tsushima Strait. Note that the seasonal variability of frontal structures can be identified. For convenience, February, May, and September represent winter, spring, and summer, respectively.

The aspect ratio (H/L; H: vertical scale; L: horizontal scale) of individual elements of finestructures is 10^{-4}–10^{-3}; that is, a finestructure with a vertical scale of few meters has approximately a horizontal scale of a few to tens kilometers. The characteristic time scale is clearly associated with the corresponding spatial scale and generally few weeks (Fedorov, 1978). The AXBT data with the horizontal spacing of 35 km and the vertical resolution of 1 m are therefore capable of detecting finestructures. The synoptic features identified from these data are realistic under the assumption that the oceanic features with a horizontal scale larger than tens kilometers persist for at least a week. Here the vertical scales of the finestructures are defined as 2−100 m because ocean features with vertical scales smaller than 1 m cannot be identified in these data. We do not examine small-scale fluctuations in surface and bottom layers, although they are related to turbulent mixing. Due to lack of concurrent salinity and velocity data and time-series data, we cannot discuss the effect of internal waves on finestructures, although the internal waves have been often observed in

the YES (Hsu *et al.*, 2000; Han *et al.*, 2001). The thermal finestructures at the thermocline depth in/around the thermal frontal zones are studied here.

3. Two Measures for Double Diffusion

There are two measures for the double-diffusive mixing. The first one is the Turner angle (Tu) (Ruddick, 1983):

$$Tu = -\tan^{-1}(R) - \frac{\pi}{4}, \quad R \equiv (\alpha d\theta / dz)/(\beta dS / dz), \tag{1}$$

where R is the density ratio, and

$$\alpha = -\frac{1}{\rho}\left(\frac{\partial \rho}{\partial \theta}\right) \quad \text{and} \quad \beta = \frac{1}{\rho}\left(\frac{\partial \rho}{\partial S}\right), \tag{2}$$

are the coefficients of thermal expansion and haline contraction. The water column is gravitationally stable for $|Tu| < \pi/4$, gravitationally unstable for $|Tu| > \pi/2$, double diffusive for $\pi/4 < Tu < \pi/2$, and the salt fingering for $-\pi/2 < Tu < -\pi/4$.

The second measure is the Cox number, which is the normalized temperature gradient variance defined by

$$C_T = \frac{Var(\Delta T_Z)}{\left(\overline{\Delta T_Z}\right)^2}, \tag{3}$$

which serves as a non-dimensional measure of finestructure intensity (Joyce, 1976). Here, $Var(\Delta T_Z)$ is the variance of vertical temperature gradient in a segment of the profile, and $\overline{\Delta T_Z}$ is the averaged vertical temperature gradient over the segment.

(need general …)

4. Detection of finestructures in frontal regions

The temperature profiles are locally grouped with respect to their vertical temperature structures related to the thermal fronts (Fig. 2) identified from these data (see Fig. 2b): Cheju-Yangtze Front (CYF), Cheju-Tsushima Front (CTF), Tsushima Front (TF), and Kuroshio Front (KF) (Park and Chu, 2007b). The CYF is two-tongue-shaped, i.e. slanted S-shaped (northern and southern tongues). The CTF occurs along the southern coast of Korea and expands between the Cheju Strait and the Korea/Tsushima Strait. The TF is a branch from the KF (Park and Chu, 2006, 2007b).

Seven groups are also identified (Fig. 2a): (1) Kuroshio Front group (KFG; in the Kuroshio Front but the Tsushima Warm Current branching region is not included), (2) Cheju−Tsushima Front group (CTFG; in the Cheju−Tsushima Front), (3) Yellow Sea Bottom Cold Water group (YCWG; northwest off the northern tongue of the CYF), (4) west of Cheju Island group (WCG; in the northern tongue of the CYF), (5) south of Cheju Island group (SCG; in northern part of the southern tongue of the CYF), (6) Yangtze Bank group (YBG), and (7) south of Yangtze Bank group (SYBG). The last two groups (YBG and SYBG) are located north and south of the western tip of the southern tongue of the CYF with consideration of seasonal migration of the southern tongue of the CYF. The SYBG also shows a thermal front induced by the Taiwan Warm Current and/or the uplifted Kuroshio northeast of Taiwan merging into the southern tongue of the CYF in summer (Park and Chu, 2007b). The forms of finestructures are diverse among these groups.

a. KFG

The staircase structure (Fig. 1a) is often found in the KFG regardless of seasons and depths except the surface mixed layer (Fig. 3) with irregular layer thickness from few to 40 meters and sheet thickness around few meters. Some staircase structures are eroded by mixing process and seen as less-defined sheets and layers. These staircase structures are called irregular-staircase (Gregg, 1975; Ruddick and Gargett, 2003) or eroded-staircase structure. This irregular-staircase structure in profiles is common in open oceans. According to Bao *et al.* (1996)'s springtime observation at the Kuroshio axis, the T–S relation is tight in irregularly-spaced layers. Profiles of the vertical temperature (salinity) gradient multiplied by the thermal expansion (haline contraction) coefficient (available at http://www.nodc.noaa.gov/) displays a good coherence between temperature and salinity variations (Fig. 4b).

When the Turner angle is calculated from the CTD data with 1 m vertical resolution, this is just a gross measure of the stability, not an actual micro-scale double diffusion (Kennan and Lukas, 1996). The halocline, from a salinity maximum (~150 m) to a salinity minimum (~500 m), lies in the salt finger regime (i.e. double diffusion) particularly in a weak fingering regime $(2 \le R < \infty)$, agreeing with the irregular-staircase structure (Fig. 4c). In the KFG 60% water column in 50−400 m depth lies in the weak fingering regime, according to Fig. 5. The double-diffusive diapycnal mixing may cause this irregular-staircase structure.

The Cox number was calculated for each profile and then averaged over the groups (Table 1; the criteria of dividing the upper KFG and the lower KFG will be explained in section 4). The Cox number in the KFG ranges from 0.3 to 0.7, which is an agreeable measure for the irregular-staircase (Hayes *et al.*, 1975; Joyce, 1976).

b. CTFG

The CTFG has highly-complex/mixed finestructures in summer, which are hardly specified as one form of the finestructure: a mixture of multiple inversions, thermocline intrusions at scales of few to 30 meters (9209 and 9309 in Fig. 6). These finestructures are overlapped on a thermocline but do not change considerably a main trend of the thermocline. They are richer in the lower part than in the upper part of the thermocline. Warm-noses (inverted structures describing maximum temperature observed between the surface mixed layer and the top of a strong thermocline) reported by Park and Chu (2007b) are seen at 10−50 m depth. The Cox number is larger than 1 in 9209 and 9309, confirming higher finestructure intensity than that in the KFG (Table 1). In 9209, a profile displays ~9^{o}C near the bottom, which is related to the Korea Strait Bottom Cold Water, the water mass passed through the Korea/Tsushima Strait from the Japan/East Sea in the bottom layer. In 9209 the cold water extends west of 129.5^{o}E along the trench of the Korea/Tsushima Strait, while in 9309 does not (see Fig. 11 in Park and Chu, 2007b).

c. YCWG and WCG

The YCWG shows smooth curves or straight lines (i.e. lack of finestructures) but a strong seasonal variability except in the bottom layer (Fig. 7). A colder layer formed above

a homogenous bottom cold layer (i.e. the Yellow Sea Bottom Cold Water) exists in 9305. No prominent finestructure except this colder layer is detected in warm seasons since the Cox numbe is quite low (~0.3) (Table 1).

The WCG is similar to the YCWG (Fig. 8) also with low Cox number (0.2−0.3). However, the WCG-9302 was separated into two groups with the occurrence of the northern tongue of the CYF. Vertical temperature–salinity–density distributions across the northern tongue (clear coherent haline and thermal fronts) show the existence of a density-compensated front (Lee *et al.*, 2003; Son *et al.*, 2003). Wintertime wind stirring suppresses the finestructure development around the northern tongue despite the homogenous density field. Nonetheless, the inversion layer at 40−70 m depth with small temperature fluctuations in WCG-9302 implies stronger cross-frontal mixing and/or advection than wind stirring (Park and Chu, 2007a). The colder layer formed above the homogenous bottom cold layer in warm seasons is not as rich as that in the YCWG.

d. SCG

The SCG is characterized by intensive summer thermocline intrusions, owing to the mixing between the modified Yellow Sea Bottom Cold Water, i.e., the water mass of 10−15°C over the Yangtze Bank extended southward from the Yellow Sea Bottom Cold Water and mixed with cold Chinese coastal water (Isobe, 1999; Furey and Bower, 2005; Park and Chu, 2006, 2007b), and the Tsushima Warm Current water (9209 and 9309 in Fig. 9). The intrusions are developed at 20−100 m depth, beneath the strong upper seasonal thermoclines, with horizontal scale of tens kilometers and vertical scale of a few to 40

meters (Park and Chu, 2007b). Especially, in the SCG-9309 temperature fluctuates with amplitude of 0.2−2°C in a range of 17−20°C at 25–80 m depth, which implies mixing between the strong upper seasonal thermocline and the bottom layer. The fluctuation in this intermediate layer seems to be linked to the homogenous water of ~18°C that splits locally the combined front of the CYF and the TF in 9309 (Park and Chu, 2007b). The intensive summer thermocline intrusions lead to the largest Cox number (4−8) within all groups (Table 1).

According to the temperature and salinity observations in June 1999 (Lee *et al.*, 2003), halocline intrusions are multilayered at rather smaller vertical scale (~10 m) in the western part of the SCG (125.5–126.5°E, ~32.5°N) in comparison with thermocline intrusions. They interpreted that these intrusions may be related to double-diffusive mixing occurring along the isopycnal surface. In their temperature and salinity observations in September 1998, haline features resemble thermal features beneath the strong upper thermoclines/haloclines, and salinity varies in-phase with temperature but rather complex. On the base of these thermohaline features, the intrusion is generated also by the vertically-sheared advection; that is, the Yangtze Diluted Water and the cold shelf water on the Yangtze Bank are advected seaward in the intermediate layer, while the Tsushima Warm Current water is advected shoreward in the bottom layer (Lee *et al.*, 2003; Park and Chu, 2007b). The thermocline intrusions are also detected in 9305 but not to greater depths. Temperature in the bottom mixed layer is the coldest in 9305, indicating southeastward

migration of the southern tongue of the CYF (Furey and Bower, 2005; Park and Chu, 2007b, 2006).

e. YBG and SYBG

The YBG shows evident thermal seasonality in the bottom mixed layer because of shallow depth and strong tidal mixing (Park and Chu, 2007a): 9−12°C in 9302, 10−12.5°C in 9305, and 22−25°C (<23ºC) in 9209 (9309) (Fig. 10). Two discernable groups of the profiles indicate the southern tongue of the CYF except in 9302. No prominent finestructure is detected. In addition, the Cox number is the lowest in the groups.

The SYBG also reveals strong horizontal thermal gradient (Fig. 11) particularly in summer, which is driven by the Taiwan Warm Current and/or Kuroshio meandering/frontal eddy-like features (Furey and Bower, 2005; Park and Chu, 2007b). The finestructure in the SYBG, however, is not as evident as that in the SCG, implying weak cross-frontal mixing. When a strong current (i.e., the Taiwan Warm Current and/or Kuroshio meander) plays a major role in frontal genesis, a cross-frontal (along-frontal) current would be weak (strong) and consequently frontal mixing would be weak as in the SYBG. On the other hand, when a weak current develops along the front, a cross-frontal current would not be negligible and consequently may induce cross-frontal mixing by thermohaline intrusions as in the SCG (Tomczak and Godfrey, 2003). Particularly, in 9209 no finestructure in the thermocline is attributable to strong winds at that time. Thick surface mixed layer pushes down the thermocline, and inhibits development of finestructures in the thermocline (Park and Chu, 2007a).

5. Spectral and statistical characteristics

Characteristics of the finestructures detected in/around the thermal fronts can be represented by vertical temperature gradient or temperature fluctuation (i.e. a high-pass-filtered or mean-removed temperature): for instance, intervals between oscillations, amplitudes of oscillations, and signs of oscillations in the vertical temperature gradient profile reveal the size and the form of finestructure (see correspondence of the temperature profile to its vertical temperature gradient in Fig. 1a). However, for data collected over the shelf shallower than 100 m, it is inappropriate to apply a high-pass-filter to such short profiles for removing larger (than the scale of finestructure) fluctuations, and therefore the vertical temperature fluctuation is not available for these data. In addition, without time series of the profiles we cannot calculate the mean-removed temperature profile accordingly. Thus, the vertical temperature gradient calculated at every vertical interval (1 m) was used to analyze the finestructure characteristics.

We conducted spectral and statistical analyses of the vertical temperature gradient ΔT_Z of locally-grouped profiles with rich finestructures (surface and bottom mixed layers were excluded in calculations): the CTFG, the SCG, and the KFG. Since the KFG contains the surface mixed layer and the seasonal thermocline at depths shallower than ~150 m, its profiles were divided into two segments: upper (upper-KFG, shallower than 150 m) and lower (lower-KFG, 151–400 m). Winter profiles with poor finestructures were excluded in the calculations (except lower-KFG).

First, ΔT_Z spectra of typical profiles of the groups were calculated to estimate the dominant size of finestructure (Fig. 12). Second, ensemble-averaged probability distribution functions (PDFs) of ΔT_Z were calculated (Fig. 13). Third, a diagram of skewness vs. interquartile-range was plotted (Fig. 14a). For the temperature gradient, the positive skewness is related to the staircase structure; the more staircase-like a profile is, the more probable low gradient values (i.e. layer) will be than high gradient values (i.e. sheet) because the low gradient occupies a larger portion of the profile (McPhaden, 1985). The interquartile-range is the difference between the 75th and the 25th percentiles of data. The large interquartile-range, i.e. the gradient spreads widely, indicates the development of any forms of finestructure except the staircase structure (the interquartile-range of the profile with rich staircase structures is small, because the low gradient (i.e. layer) occupies a larger portion of the profile). Most summer profiles present large interquartile-range (Fig. 14a). Fig. 14a shows four zones (zone-1 to zone-4) according to finestructure characteristics. The zoning histogram shows the profile occurrence percentage of each zone (Fig. 14b). More explanations of the zones will be given later. Fourth, a diagram of the Cox number vs. gradient ratio was plotted (Fig. 15a). The gradient ratio is defined as the occurrence of $\Delta T_Z \le 0$ (i.e. inverted or isothermal layer) divided by that of $\Delta T_Z > 0$ (i.e. layer where temperature decreases with depth) over the segment. For example, when one third of all ΔT_Z calculated at every vertical interval over the segment is non-positive and the rest is positive, the gradient ratio is 0.5. The larger the Cox number (or the gradient

ratio), the higher the potential for mixing is. The intensity and the form of finestructure can be represented by the Cox number–gradient ratio diagram by three zones, zone-α to zone-γ, (Fig. 15a) and corresponding occurrence (Fig. 15b).

According to our calculation for the four groups, the zone-α exhibits the irregular-staircase with the Cox number <0.7 and the gradient ratio <~0.1; two critical values (Cox number = 0.7; gradient ratio = 0.1) are indicated in Fig. 15a. Our range of the Cox number for the irregular-staircase is consistent to several earlier studies (Hayes *et al.*, 1975; Joyce, 1976). The profiles of zone-α generally have low interquartile-range (<0.1) and high skewness (~2); two critical values (interquartile-range = 0.1; skewness = 2) are indicated in Fig. 14a. Additionally, some of these profiles show even lower interquartile-range, so that a lower critical value (interquartile-range = 0.05, marked in Fig. 14a) divides the zone-1 and the zone-2. More staircase-like profiles, i.e. thicker layer of the stair, would fall in zone 3. The zone-β shows the thermocline intrusion with the Cox number > 1 and the gradient ratio ~1. The profiles of zone-β generally have higher interquartile-range and lower skewness than the profiles of zone-α (irregular-staircase) (Fig. 14a; zone-4). The zone-γ is an intermediate zone between zone-α and zone-β (with partially overlapping with them). Profiles have less typical characteristics in the zone-γ than in either zone-α or zone-β.

A well-defined staircase structure is expected to have the Cox number >1 and the gradient ratio$\gg$1. This was not detected in the AXBT data, though. Even in zone-4, a

profile could have the zone-α features if the mean gradient of thermocline is large (e.g. some profiles in CTFG). The two diagrams should therefore be considered together.

a. Upper Segment of KFG

The spectra of the vertical temperature gradient in the upper segment show a distinct seasonal variability in all vertical wavenumbers (Fig. 12a). In the summer a dominant size of the finestructure is 10−20 m with the peak at 0.05−0.1 cycles per meter (cpm) (Fig. 12a). For $\Delta T_Z > 0.05$°C m^{-1}, the probability of the vertical temperature gradient enhances from winter to summer (Fig. 13a). Since this high gradient is consistent with the gradient of the sheets (~0.1°C m^{-1}) in the KFG, the development of the staircase structure is responsible for the gradient enhancement. In the summer, the zone-2 occurs more often in the upper-KFG than in the lower-KFG (Fig. 14b), which causes larger interquartile-range in the upper-KFG than in the lower-KFG. This implies that the finestructure scale and/or form tend to have more variability in the upper-KFG than in the lower-KFG. For the zone-3, profiles are more staircase-like (thicker layer in the stair) in 9309 than in 9209 (Fig. 14b). In the spring there is no significant difference in the finestructure between the upper and the lower segments in terms of spectra and statistics, owing to the absence of seasonal thermocline (9305 in Figs. 12a, 13a; 9305 in Figs. 12b, 13b; 9305 in Figs. 14b, 15b).

b. Lower Segment of KFG

In contrast to the upper-KFG, the spectra of the vertical temperature gradient in the lower segment are almost seasonally invariant regardless of seasonal temperature variability (Figs. 3, 12b). The seasonal invariance of the finestructure is also confirmed by

the PDFs (see four very similar curves in Fig. 13b) and the two zoning histograms (see resemblance of bars to each survey in Figs. 14b, 15b). In the winter, the surface mixed layer deepening affects the finestructure slightly through increasing zone-3 (zone-γ) in 9202 compared with the other surveys as shown in Fig. 14b (Fig. 15b).

A significant occurrence percentage, 60-~80%, of zone-1 (zone-α) in Fig. 14b (Fig. 15b) demonstrates the dominance of staircase structure. The slope of the spectra is gentle (~10^{-2}) in high vertical wavenumbers (>10^{-1} cpm) (Fig. 12b). The Cox number of the lower-KFG is lower than that of the CTFG and the SCG (Fig. 15a). These spectral and statistical features suggest that mixing in the lower-KFG is more frequent at vertical scales <10 m than at vertical scales >10 m, but is not as vigorous as in the CTFG and the SCG.

c. CTFG

The energy level of the spectra of the vertical temperature gradient is $10^{1.0}$-$10^{1.5}$ times higher in the summer than in the spring (Fig. 12c). In the summer, the PDFs of vertical temperature gradient display a low peak with a long irregular tail toward the large vertical gradient (Fig. 13c), evidencing the complex/mixed finestructures at scales of a few to 30 meters mentioned in section 3b. This PDF is contrasted to a high peak with a short smooth tail of all-season lower segment of the KFG (Fig. 13b). A dominant mixing mechanism could therefore be different between the CTF and the KF. Note that the CTF is lack of one-zone-dominancy unlike the other groups (Figs. 14b, 15b). The region around the CTF is a confluence area of various water masses: the water mass transported by the Tsushima Warm Current, the water mass passed through the Cheju Strait, the water mass

along the south coast of Korea, and the water mass passed through the Korea/Tsushima Strait in the bottom layer. The mixing among those water masses is complicated and mixing scale varies widely.

d. SCG

The PDFs of vertical temperature gradient in the SCG are similar as in the CTFG, i.e. the low peak with the long irregular tail toward to the large gradient (Fig. 13d). However, the PDFs in the SCG show higher percentage in the negative to zero gradient range than those in the CTFG; especially in the summer the probability of the vertical gradient in this range increases by ~45%. Similarly the gradient ratio is nearly one, highest in the YES (Fig. 15a). The Cox number is also the highest. Accordingly, zone-β occurs more often in the SCG than in the CTFG (Fig. 15b). More than 60% of the SCG profiles belong to zone-4, unlike the other groups (Fig. 14b). These features are associated with thicker uniform and/or inversion layers in the SCG, which result from the temperature fluctuation between the strong upper seasonal thermoclines and the bottom layer as mentioned in section 3d and yield more vigorous mixing than the CTFG. Scale and magnitude of the vertical temperature fluctuation are also greater in the SCG than in the CTFG (Figs. 6, 9). In the SCG the peaks of spectra are located at vertical wavenumbers $< 5\times10^{-2}$ cpm, i.e. vertical scales > 20 m (Fig. 12d). These finestructure characteristics of the SCG are consistent with the greatest cross-frontal heat flux and lateral eddy diffusivity in the YES (Park and Chu, 2007b).

6. Finestructures in the Tsushima Warm Current branching region

a. Horizontal incoherency

The Tsushima Warm Current branching occurs generally in 127–128°E and 30°N. The warm saline water detached from the Kuroshio flows onto the ECS shelf, despite seasonal variations (Huh, 1982; Lie *et al.*, 1998; Hsueh, 2000; Furey and Bower, 2005) (Fig. 16). In the warm seasons the Tsushima Warm Current connects to the southern tongue of the CYF and is contributed by the Taiwan Warm Current (Isobe, 1999; Ichikawa and Beardsley, 2002; Furey and Bower, 2005; Park and Chu, 2007b). Just apart from the branching location, meanders and eddies often occur (Lie *et al.*, 1998; Nakamura *et al.*, 2003) and bottom relief is complex (Fig. 16). Mesoscale eddy stirring can create finestructures, which are characterized by lack of horizontal coherency (Ferrari and Polzin, 2005). For these reasons the temperature profiles in the Tsushima Warm Current branching region are horizontally less coherent than those in the KFG (Fig. 17; Fig. 2 by Yang *et al.*, 2004). Here, for convenience the branching region is assumed wider to encompass the branching location. In particular, this horizontal incoherency is obvious in 9302 and 9305. Hence, finestructure characteristics here need to be analyzed by individual profiles, rather than by their ensemble-averages.

b. Comparison of profiles on and off the branching location

We analyzed individual profiles in three stations (Figs. 18, 19). One of them was approximately in the branching location (Stn-A; 128.0°E, 29.7°N), and two others were a little north (Stn-B; 127.6°E, 30.8°N) and south (Stn-C; 128.6°E, 29.0°N) of the branching

location in order to compare finestructures on and off the branching location (Fig. 16). The south (north) station of the branching location presents a profile before (after) the branching.

At Stn-B, the subsurface Kuroshio water (<21ºC, >24.4 σ_θ; Oka and Kawabe, 1998) intrudes onto the shelf at depths deeper than 100 m all the year and sustains temperature of 16−17°C in the bottom layer (Stn-B in Fig. 18a). For 9305 and 9309 there is a big jump in the intermediate layer (~75 m depth) in the vertical temperature gradient and its cumulative variance (cumulate variance from the surface to every depth of the profile) (Stn-B in Figs. 18b, c). This jump implies that different water masses meet and mix. At Stn-C, on the other hand, weak gradient exhibits (Stn-C in Fig. 18b). The cumulative variance of the gradient at Stn-C is less than one sixth of that at Stn-B, as compared at 130 m depth (Stn-C in Fig. 18c). The energy spectra of the vertical temperature gradient at Stn-C (except 9302) are also 10^1−10^2 times lower than those at Stn-B, especially much lower in the low (<10^{-1} cpm) vertical wavenumbers (Fig. 19). These spectral and statistical characteristics imply poor finestructures at a vertical scales >10 m at Stn-C in comparison to that at Stn-B.

In the summer, large (10–50 m thick) irregular-staircase structures are strong with big jumps in the gradient and the large cumulative variance of the gradient in the upper part (shallower than 230 m) of Stn-A and Stn-B (Figs. 18a–c) but not of Stn-C. The PDFs of vertical temperature gradient of Stn-A and Stn-B have the second peak at 0.25ºC m^{-1} (corresponding to the sheets) (Fig. 18d). In contrast, the large irregular-staircase structure is

comparatively weak in the deeper part (deeper than 230 m) of Stn-A, which is similar to Stn-C.

The energy spectra of the vertical gradient resemble in shape and slope between Stn-A and Stn-C in the high vertical wavenumbers (>10^{-1} cpm), and are higher in Stn-A than in Stn-C in the low vertical wavenumbers (<10^{-1} cpm) (9209 and 9309 in Fig. 19, although 9309 does not show these feature as clearly as 9209). Peaks at ~0.02 cpm (0.05–0.1 cpm) seem to be related to the size of layers (sheets) (9209 and 9309 in Fig. 19-Stn A).

c. Generation mechanism

Since the cold Kuroshio subsurface water is uplifted at Stn-A, temperature of Stn-A is colder than that of Stn-C at depths deeper than 100 m (Fig. 18a). This uplifted cold water and the cold shelf water cause strong horizontal temperature gradient against the warm Kuroshio surface water (>21ºC) (Oka and Kawabe, 1998; Su and Wang, 1994), and this gradient accordingly induces the large irregular-staircase structure in the upper part of Stn-A. The development of the large irregular-staircase structure is confirmed by the difference of Stn-A and Stn-C in the spectra and statistics mentioned in Section 6b.

This strong horizontal gradient seems to be formed also in salinity field and then develop an irregular halocline structure, although we do not have concurrent salinity data. According to the springtime temperature and salinity profiles in Bao *et al.* (1996, see their Fig. 2), which are close to Stn-A, salinity varies generally in phase with temperature and presents rich multilayered structures in the profiles at shallower than ~200 m depth. Salinity (temperature) varies in the range of 0.5–1 psu (1–2ºC) in a sheet with thickness <10 m. In

addition, the vertical salinity distributions in the branching region observed in May 1995 present a variety of finestructures, such as low or high cores and multilayered structures, in 10–50 km long and a few to tens meters thick according to Lie *et al.* (1998, see their Fig. 6). It is noted that the lower limit of these finestructures (~200 m depth) generally coincides with the depth of maximum salinity zone (~34.7 psu) and seasonal pycnocline, based on their observations and GDEM data. Fig. 4 also presents this feature, although the profile is in the KFG. No prominent finestructure except the staircase is below 200 m, like in Stn-C and the lower segment of the KFG (Fig. 18c): the finestructure develops down to minimum salinity zone (~700 m depth), and it is nearly seen beyond the zone (Fig. 4).

The thermal and density fronts generated by the Tsushima Warm Current branching are coherent in vertical distributions of temperature and density, whereas the corresponding haline front, narrower than the thermal or density front, is located close to the shoreward boundary of the thermal or density front. Such haline finestructures as mentioned above are enriched in the seaward side away from the haline front, but still inside the thermal/density frontal zone, following isopycnal surfaces (Lee *et al.*, 2003). Taking these features into account, the thermohaline structures tend to be compensated in the branching region, consistent to Bao *et al.*, (1996). The effect of temperature on density, however, seems to be greater than that of salinity, although richer finestructures in their studies are detected in the salinity field and salinity compensates or dominates density locally and often above the maximum salinity zone.

7. Conclusions

The four AXBT surveys were used to analyze thermal finestructures and their seasonality in frontal zones of the southern Yellow Sea and the East China Sea. The possible mechanisms for generating these finestructures were discussed. For the lack of concurrent salinity/velocity and time series data, only limited analyses on temperature were possible. The four surveys conducted in one year are not quantitatively sufficient to describe the finestructure seasonality with robust statistics. However, with a good synoptic view of the AXBT data, we demonstrated that the finestructure characteristics are different not only among the fronts but also along the front, suggesting that different mixing mechanisms are related. The results are summarized as follows:

(1) The thermal finestructure in the Kuroshio Front is characterized by the irregular-staircase consisting of alternative sheets (a few meters thick with a gradient of ~0.1°C m^{-1}) and layers (a few to 40 m thick). The lower (151–400 m) segment of the Kuroshio Front Group reveals seasonal invariance in finestructure, unlike the upper segment (shallower than 150 m). The winter surface mixed layer deepening, however, makes the layer of the irregular-staircase rather thicker. The vertical temperature gradient in the range of $0 < \Delta T_Z \leq 0.05$ °C m^{-1} accounts for 70% of its distribution probability in all seasons, implying that single mixing mechanism (probably double diffusive diapycnal mixing) is dominant in generating the finestructure. The Cox number is lower in the Kuroshio Front than in the Cheju–Tsushima Front or the northeastern part of the southern tongue of the Cheju–Yangtze Front, and the scale of finestructure is comparatively smaller.

(2) The temperature profiles in/around the Cheju–Tsushima Front reveal highly complex/mixed finestructures at the scales of a few to 30 meters in the lower part of the thermocline in the summer. This finestructure characteristic is confirmed by the low peak with a long irregular tail in the PDF of the vertical temperature gradient as well as the lack of one-zone-dominancy in the statistical classifications by finestructure characteristics. Since the Cheju–Tsushima Front region is the confluence area in the YES crowded with water masses from different origins, mixing among these water masses is likely to occur in many ways and to yield such complex/mixed finestructures.

(3) The northern tongue of the Cheju–Yangtze Front shows no prominent finestructures except the colder layer formed above the homogenous bottom cold layer in warm seasons. Occurrence of winter inversion layer at 40−70 m depth with small temperature fluctuations indicates sufficiently strong cross-frontal mixing and/or advection to overcome the wind stirring.

(4) The thermal finestructure along the southern tongue of the Cheju–Yangtze Front has large variability locally. In the northeastern part of the southern tongue (south of Cheju Island), it is characterized by summer intensive thermocline intrusions at the horizontal scales of tens kilometers and the vertical scales of a few to 40 m. Similar but smaller-scale haline finestructure was also observed in this region (Lee *et al.*, 2003). These thermohaline finestructures may be driven by the vertically-sheared advection. In addition, Lee *et al.* (2003) suggested that both double-diffusive process along isopycnal surface and baroclinity should be taken into account. These intrusions, exhibiting large Cox number,

large gradient ratio, and large interquartile-range, contributes large lateral mixing related to weak horizontal density gradient, great cross-frontal heat flux, and great lateral eddy diffusivity (Lee *et al.*, 2003; Park and Chu, 2007b).

On the other hand, the finestructure in/around the southwestern part of the southern tongue (southern Yangtze Bank) is not as rich as that in/around the northeastern part in warm seasons. This is attributed to weak cross-frontal mixing around the front, which is mainly caused by strong along-frontal currents, such as the Taiwan Warm Current and/or the Kuroshio meandering.

(5) The profiles in the Tsushima Warm Current branching region are different even locally, and such difference is more distinctive in the spring. The profile on the branching location displays larger irregular-staircase thermocline (at vertical scale of 10–50 m) in the upper part (shallower than 230 m, like the profiles north of the branching location) than in the lower part (like the profiles south of the branching location). The strong horizontal temperature gradient between the uplifted cold subsurface Kuroshio water/the cold shelf water and the warm Kuroshio surface/near-surface water is the source to develop this large irregular-staircase. Related haline finestructure, which is more multilayered, is seen in several studies (Bao *et al.*, 1996; Lie *et al.*, 1998; Lee *et al.*, 2003). The front in this region is partially density-compensated. The lower bound of these thermohaline finestructures (~200 m depth) generally coincides with the depth of maximum salinity zone (~34.7 psu) and seasonal pycnocline.

Acknowledgments

This research was sponsored by the Naval Oceanographic Office, Office of Naval Research, and Naval Postgraduate School.

References

Bao, X.-W., X.-H. Fang, and X.-G. Liu (1996): Thermohaline finestructure and its relation with the water masses and currents system in the northern East China Sea. *Chin. J. Oceanol. Limnol.*, **14**(2), 122–128.

Bianchi, A. A., C. F. Giulivi, and A. R. Piola (1993): Mixing in the Brazil-Malvinas confluence. *Deep Sea Res.*, **40**(7), 1345–1358.

Boyd, J.D., and R.S. Linzell (1993): Evaluation of the Sparton tight-tolerance AXBT. *J. Atmos. Oceanic Technol.,* **10**, 892-899.

Boyer, T. P., and S. Levitus (1994): Quality control and processing of historical temperature, salinity, and oxygen data. NOAA Technical Report NESDIS 81.

Chu, P.C., S.K. Wells, S.D. Haeger, C. Szczechowski, and M. Carron (1997a): Temporal and spatial scales of the Yellow Sea thermal variability. *J. Geophys. Res*., 102, 5655-5668.

Chu, P.C., C.R. Fralick, S.D. Haeger, and M.J. Carron (1997b): A parametric model for Yellow Sea thermal variability. *J. Geophys. Res*., 102, 10499-10508.

Chu, P.C., Y.C. Chen, and A. Kuninaka (2005): Seasonal variability of the East China/Yellow Sea surface buoyancy flux and thermohaline structure. *Adv. Atmos. Sci*., 22, 1-20.

Chu, P.C., H.C. Tseng, C.P. Chang, and J.M. Chen (1997): South China Sea warm pool detected from the Navy's Master Oceanographic Observational Data Set (MOODS), *J. Geophys. Res*., 102, 15761-15771.

Chu, P.C., C.W. Fan, C.J. Lozano, and J. Kerling (1998): An airborne expandable bathythermograph survey of the South China Sea, May 1995. *J. Geophys. Res*., **103**, 21637-21652.

Fedorov, K. N. (1978): *The thermohaline finestructure of the ocean.* translated by D. A. Brown, technically edited by J. S. Turner, 170pp, Pergamon Press.

Ferrari, R., K. L. Polzin (2005): Finescale structure of the T–S relation in the Eastern North Atlantic. *J. Phys. Oceanogr.*, **35**, 1437–1454.

Furey, H., and A. Bower (2005): The synoptic temperature structure of the East China and southeastern Japan/East Seas. *Deep Sea Res. II*, **52**, 1421–1442.

Georgi, D. T. (1978): Finestructure in the Antarctic Polar Front Zone: its characteristics and possible relationship to internal waves. *J. Geophys. Res.*, **83**, 4579–4588.

Georgi, D. T. (1981): On the relationship between the large-scale property variations and fine structure in the Circumpolar Deep Water. *J. Geophys. Res*., **86**, 6556–6566.

Georgi, D. T. (1975): Variations in the intensity of small-scale mixing in the main thermocline. *J. Phys. Oceanogr.*, **5**, 253–278.

Gregg, M. C. (1977): Variations in the intensity of small-scale mixing in the main thermocline. *J. Phys. Oceanogr.*, **7**, 436–454.

Han, I-S., K. Kamio, T. Matsuno, A. Manda, and A. Isobe (2001): High frequency current fluctuations and cross shelf flows around the pycnocline near the shelf break in the East China Sea. *J. Oceanogr.*, **57**, 235–249.

Hayes, S. P., T. M. Joyce, and R. C. Millard (1975): Measurements of vertical fine structure in the Sargasso Sea. *J. Geophys. Res.*, **80**, 314–319.

Hsu, M.-K., A. K. Liu, and C. Liu (2000): A study of internal waves in the China Seas and Yellow Sea using SAR. *Cont. Shelf Res.*, **20**, 389–410.

Hsueh, Y. (2000): The Kuroshio in the East China Sea. *J. Mar. Sys.*, **24**, 131–139.

Huh, O. K. (1982): Spring-season flow of the Tsushima Current and its separation from the Kuroshio: satellite evidence. *J. Geophys. Res.*, **87**, 9687–9693.

Ichikawa, H., and R. C. Beardsley (2002): Review: The current system in the Yellow and East China Seas. *J. Oceanogr.*, **58**(1), 77–92.

Isobe, A. (1999): The Taiwan-Tsushima Warm Current system: its path and the transformation of the water mass in the East China Sea. *J. Oceanogr.*, **55**(2), 185–195.

Jugan, M.J., and H. Beresford (1992): Editing approach for the Navy's Master Oceanographic Observation Data Set. *Proceed. of MTS '91, An Ocean Cooperative: Industry, Government, and Academia*. 1164.

Joyce, T. M (1976): Large-scale variations in small-scale temperature/salinity finestructure in the main thermocline of the northwest Atlantic. *Deep Sea Res. II*, **23**, 1175–1186.

Kennan, S. C., and R. Lukas (1996): Saline intrusions in the intermediate waters north of Oahu, Hawaii. *Deep Sea Res. II*, **43**, 215−241.

Lee, J.-H., and K. Richards (2004): The three-dimensional structure of the interleaving layers in the western equatorial Pacific Ocean. *Geophys. Res. Lett.*, **31**, L07301, doi:10.1029/2004GL019441.

Lee, J.-H., H.-J. Lie, and C.-H. Cho (2003): The structure of ocean fronts in the East China Sea. *Proceed. of the 12th PAMS/JECSS Workshop*, Hangzhou, China. 2-10-1~2.

Lie, H.-J., C.-H. Cho, and J.-H. Lee (1998): Separation of the Kuroshio water and its penetration onto the continental shelf west of Kyushu. *J. Geophys. Res.*, **103**, 2963–2976.

Lie, H.-J., C.-H. Cho, and J.-H. Lee, and S. Lee (2003): Structure and eastward extension of the Changjiang River plume in the East China Sea. *J. Geophys. Res.*, **108**, 3077, doi:10.1029/2001JC001194.

Lie, H.-J., C.-H. Cho, and J.-H. Lee, S. Lee, and Y. Tang (2000): Seasonal Variation of the Cheju Warm Current in the Northern East China Sea. *J. Oceanogr.*, **56**(2), 197-211.

McPhaden, M. J. (1985): Fine-structure variability observed in CTD measurements from the central equatorial Pacific. *J. Geophys. Res.*, **90**, 11726–11740.

Nakamura, H., H. Ichikawa, A. Nishina, and H.-J. Lie (2003): Kuroshio path meander between the continental slope and the Tokara Strait in the East China Sea, *J. Geophys. Res.*, **108**(C11), 3360, doi:10.1029/2002JC001450.

Nandi, P., W. S. Holbrook, S. Pearse, P. Paramo, and R. W. Schmitt (2004): Seismic reflection imaging of water mass boundaries in the Norwegian Sea. *Geophys. Res. Lett.*, **31**, L23311, doi:10.1029/2004GL021325.

Oka, E., and M. Kawabe (1998): Characteristics of variations of water properties and density structure around the Kuroshio in the East China Sea. *J. Oceanogr.*, **54**, 605–617.

Park, S., and P. C. Chu (2006): Thermal and haline fronts in the Yellow/East China Seas: surface and subsurface seasonality comparison. *J. Oceanogr*., **62**, 617–638.

Park, S., and P. C. Chu (2007a): Synoptic distributions of thermal surface mixed layer and thermocline in the southern Yellow and East China Seas. *J. Oceanogr*., **63**, 1021−1028.

Park, S., and P. C. Chu (2007b): Synoptic frontal structures and cross-frontal heat fluxes in the southern Yellow Sea and East China Sea. *Acta Ocenologica Sinica* (accepted).

Peters, H., M. C. Gregg, and T. B. Sanford (1991): Equatorial and off-equatorial fine-scale and large-scale shear variability at 140°W. *J. Geophys. Res.*, **96**, 16913–16928.

Richards, K., and H. Banks (2002): Characteristics of interleaving in the western equatorial Pacific. *J. Geophys. Res.*, **107**, 3231, doi:10.1029/2001JC000971.

Ruddick, B. (1983): A practical indicator of the stability of the water column to double-diffusive activity. *Deep Sea Res.*, **30,** 1105−1107.

Ruddick, B., and A. E. Gargett (2003): Oceanic double-infusion: introduction. *Progress in Oceanogr.*, **56**, 381–393.

Ruddick, B., and K. Richards (2003): Oceanic thermocline intrusions: observation. *Progress in Oceanogr.*, **56**, 499–527.

Schmitt, R. W., and D. T. Georgi (1982): Finestructure and microstructure in the North Atlantic Current. *J. Marine Res.*, **40**, 659–705.

Schmitt, R. W., R. G. Lueck, and , T. M. Joyce (1986): Fine- and micro-structure at the edge of a warm core ring. *Deep-Sea Res.*, **33**, 1665–1689.

Schmitt, R. W., H. Perkins, J. D. Boyd, and M.C. Stalcup (1987): C-SALT: An investigation of the thermohaline staircase in the western tropical North Atlantic. *Deep-Sea Res.*, **34**, 1655–1665.

Son, Y.-T., S.-H. Lee, J. C. Lee, and J.-C. Kim (2003): Water masses and frontal structures in winter in the northern East China Sea. *J. Korean Soc. Oceanogr. (The Sea)*, **8**(3), 327─339 (in Korean with English abstract).

Su, Y.-S., and X.-C. Weng (1994): Water masses in China Seas. *Oceanology of China Seas*, vol.1, Zhou, Y.-B. Liang, and C. K. Tseng, Ed., Kluwer Academic Publishers, 3–16.

Teague, W. J. (1986): A technique for processing noisy AXBT (Airborne Expendable Bathythermograph) data. NAVOCEANO Technical Report, 17pp.

Tomczak M., and J. S. Godfrey (2003): *Regional Oceanography: an Introduction*, Daya Publishing House, 390 pp.

Toole, J.M. (1981): Intrusion characteristics in the Antarctic Polar Front. *J. Phys. Oceanogr.*, **11**, 780–793.

Warren, B. A., and C. Wunsch (1981): *Evolution of Physical Oceanography*. MIT Press, 623 pp.

Williams, A. J. (1981): The role of double-diffusion in a Gulf Stream frontal intrusion. *J. Geophys. Res.*, **86**, 1917–1928.

Yang, J., S. Zhou, J.-X. Zhou, and J. F. Lynch (2004): Internal wave characteristics at the ASIAEX site in the East China Sea. *IEEE J. Oceanic Eng.*, **29**, 1054–1060.

Zodiatis, G., and G. P. Gasparini (1996): Thermohaline staircase formations in the Tyrrhenian Sea. *Deep-Sea Res.*, **43**, 655-678.

Figure captions

Figure 1. Various finestructures: (a) a staircase (profile 1 observed at 126.3°E, 27.0°N), (b) a thermocline intrusion (profile 2 at 127.1°E, 32.8°N; profile 3 at 126.3°E, 32.8°N), (c) mixed structures (profile 4 at 128.4°E, 34.1°N; profile 5 at 127.2°E, 33.6°N; profile 6 at 127.1°E, 31.8°N). See details in the text. A thin black curve in (a) is the vertical temperature gradient of profile-1 and its scale is on the top of the figure. An inside figure of (a) is an enlargement of the segment (200–250 m) of the temperature of profile-1.

Figure 2. (a) Four airborne expendable bathythermograph (AXBT) surveys conducted on 18–29 September 1992 (9209), 4–14 February 1993 (9302), 5–14 May 1993 (9305) and 2–10 September 1993 (9309). Contours indicate the bottom bathymetry shallower than 1000 m. Seven grey boxes indicate locally-grouped profiles: Yellow Sea Bottom Cold Water group (YCWG), west of Cheju group (WCG), south of Cheju group (SCG), Cheju-Tsushima Front group (CTFG), Yangtze Bank group (YBG), south of Yangtze Bank group (SYBG), and Kuroshio Front group (KFG). (b) Identified thermal fronts with a temperature distribution at 25 m depth from the AXBT surveys: Cheju-Yangtze Front (CYF), Cheju-Tsushima Front (CTF), Tsushima Front (TF), and Kuroshio Front (KF) (Park and Chu, 2007b).

Figure 3. Temperature profiles in KFG (location see Fig. 2a).

Figure 4. (a) A temperature/salinity profile observed at 127.14^{o}E and 28.25^{o}N in June 1994, provided by WOD05: a back (gray) line for temperature (salinity), (b) A vertical temperature/salinity gradient from the profiles of (a): a back (gray) line for temperature

(salinity). A horizontal axis (a unit 10^{-5} m) was scaled by the thermal expansion and haline contraction coefficients so that the fluctuations of temperature and salinity gradients of equal size imply identical effects on density. (c) Turner angle of from the profiles of (a): see details in the text. The density ratio *R* corresponding to the Turner angle is marked at the top.

Figure 5. A histogram of the Turner angle calculated from 260 profiles (51−400 m) in KFG: the profiles data were extracted from WOD05 for a period of 1991−2002. A bin size is $\pi/50$. The density ratio *R* corresponding to the Turner angle is marked at the top.

Figure 6. Temperature profiles in CTFG (see Fig. 2a).

Figure 7. Temperature profiles in YCWG (see Fig. 2a).

Figure 8. Temperature profiles in WCG (see Fig. 2a).

Figure 9. Temperature profiles in SCG (see Fig. 2a).

Figure 10. Temperature profiles in YBG (see Fig. 2a).

Figure 11. Temperature profiles in SYBG (see Fig. 2a).

Figure 12. Spectra of vertical temperature gradient in the groups. KFG is divided into upper segment (upper-KFG, shallower than 150m) and lower segment (lower-KFG, 151−400 m).

Figure 13. Ensemble-averaged PDFs of vertical temperature gradient in the same groups as in Fig. 10. Marks are placed at the center of bin with a size of 0.05 °C m^{-1}.

Figure 14. (a) A diagram of interquartile-range vs. skewness of vertical temperature gradient in the same groups as in Fig. 10 (see details in the text). The diagram is divided into four zones: zone-1 (interquartile-range ≤ 0.05 and skewness ≤ 2), zone-2

(0.05 < interquartile-range ≤ 0.1 and skewness ≤ 2), zone-3 (skewness > 2), and zone-4 (interquartile-range > 0.1 and skewness ≤ 2). (b) A histogram of profile population percentage of the four zones.

Figure 15. (a) A diagram of Cox number vs. gradient ratio of vertical temperature gradient in the same groups as in Fig. 10 (see details in the text). The diagram has three zones: zone-α (Cox number ≤ 0.7 and gradient ratio ≤ 0.1), zone-β (Cox number > 0.7 and gradient ratio > 0.1), and zone-γ (0.5 < Cox number ≤ 2 and 0.05 < gradient ratio ≤ 0.5). (b) A histogram of profile population percentage of the three zones.

Figure 16. Systematic of the current system in the East China Sea. The Kuroshio following along the continental shelf is separated into the northern branch, i.e. the Tsushima Warm Current, and the eastern northern branch at 127–127°E and 29–30°N, which is assumed as the Tsushima Warm Current branching location (Huh, 1982; Lie *et al.*, 1998; Hsueh, 2000; Furey and Bower, 2005). The Taiwan Warm Current, which passes through the Taiwan Strait and then flows over the continental shelf, contributes to the Tsushima Warm Current in warm seasons (Isobe, 1999; Ichikawa and Beardsley, 2002). The AXBT stations are marked by a cross. Three individual AXBT profiles marked by an open circle are used for calculating spectral and statistical values in the Tsushima Warm Current branching region: a station at the branching location labeled by "A" and the two neighboring stations labeled by "B" and "C" (Stn-A, Stn-B, and Stn-C, respectively). A box is for Fig. 17.

Figure 17. Temperature profiles in the Tsushima Warm Current branching region (a box in Fig. 16).

Figure 18. Temperature profiles (a), vertical temperature gradient (b), cumulative variance of vertical temperature gradient (c), and distribution probability of vertical temperature gradient (d) of three stations in the Tsushima Warm Current branching region (see Fig. 16; Stn-A for the first row, Stn-B for second, and Stn-C for third). In (b) and (c) 9209 is correct for scale at top and remaining curves are offset by 0.5 ºC m^{-1} and 1 $ºC^2$ m^{-2}, respectively.

Figure 19. Spectra of vertical temperature gradient of the three stations in the Tsushima Warm Current branching region (see Fig. 16).

1 Table 1. Cox number averaged over the group.

	9209	9302	9305	9309
Upper KFG	0.32	0.44	0.40	0.62
Lower KFG	0.36	0.43	0.43	0.40
CTFG	1.10		0.51	1.62
YCWG	0.28		0.35	0.33
WCG	0.22		0.21	0.26
SCG	7.91		0.56	4.54
YBG	0.09		0.20	0.23
SYBG	0.13		0.24	0.28

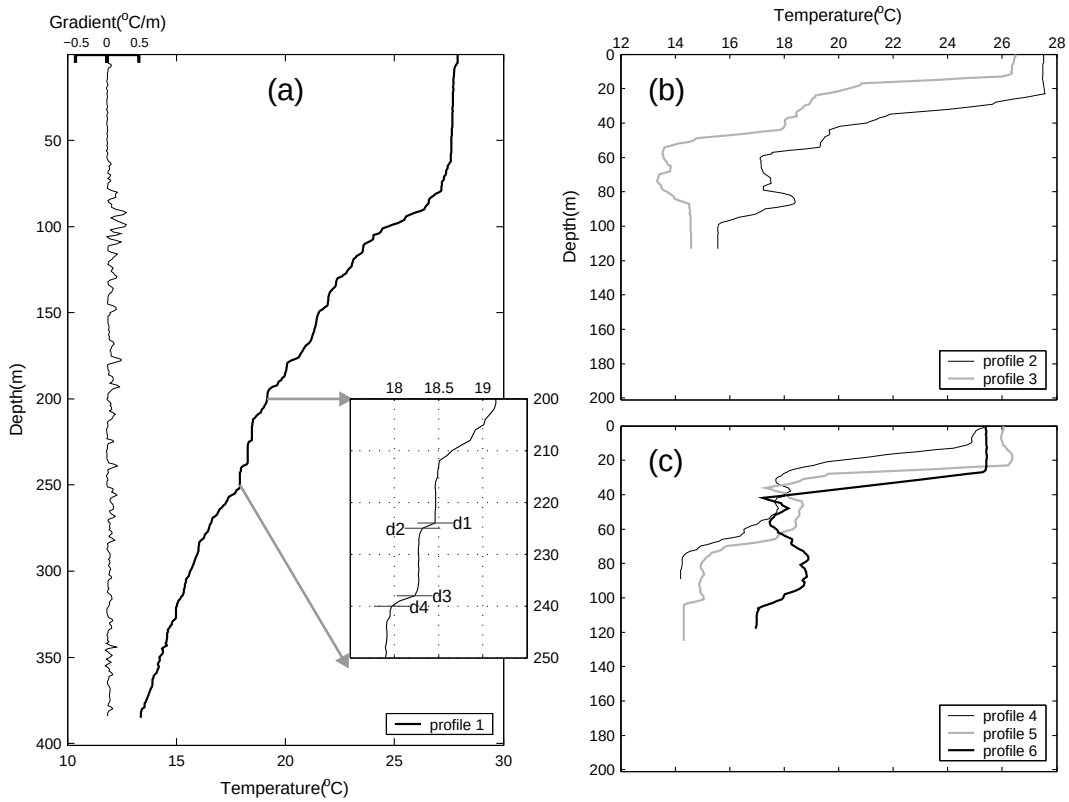

Figure 1. Various finestructures: (a) a staircase (profile 1 observed at 126.3°E, 27.0°N), (b) a thermocline intrusion (profile 2 at 127.1°E, 32.8°N; profile 3 at 126.3°E, 32.8°N), (c) mixed structures (profile 4 at 128.4°E, 34.1°N; profile 5 at 127.2°E, 33.6°N; profile 6 at 127.1°E, 31.8°N). See details in the text. A thin black curve in (a) is the vertical temperature gradient of profile 1 and its scale is on the top of the figure. An inside figure of (a) is an enlargement of the segment (200–250 m) of the temperature of profile 1.

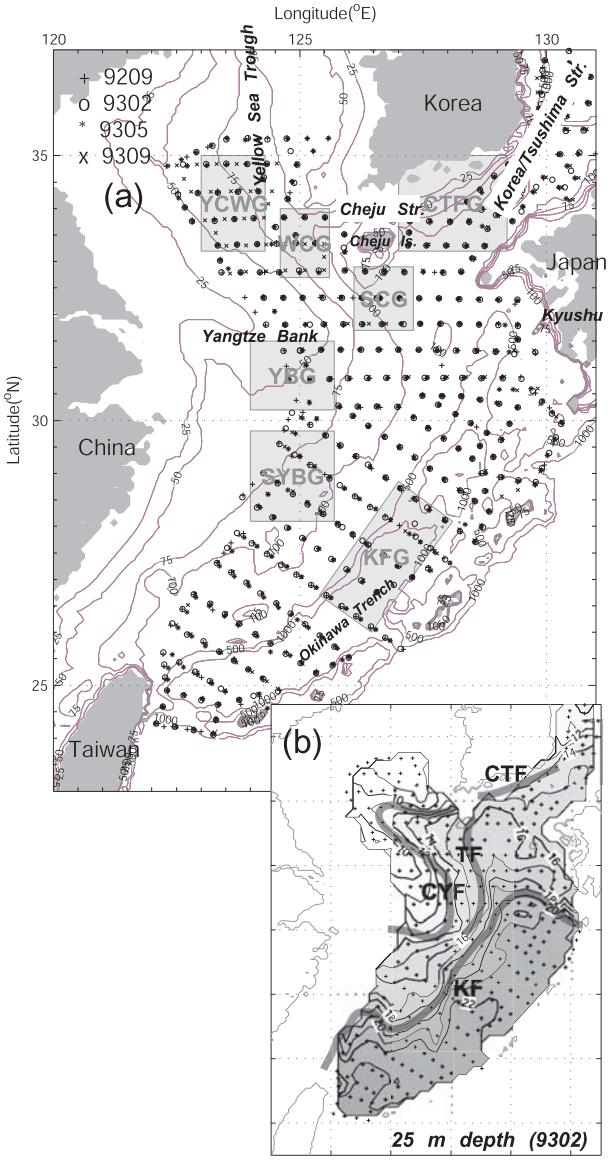

Figure 2. (a) Four airborne expendable bathythermograph (AXBT) surveys conducted on 18–29 September 1992 (9209), 4–14 February 1993 (9302), 5–14 May 1993 (9305) and 2–10 September 1993 (9309). Contours indicate the bottom bathymetry shallower than 1000 m. Seven grey boxes indicate locally-grouped profiles: Yellow Sea Bottom Cold Water group (YCWG), west of Cheju group (WCG), south of Cheju group (SCG), Cheju-Tsushima Front group (CTFG), Yangtze Bank group (YBG), south of Yangtze Bank group (SYBG), and Kuroshio Front group (KFG). (b) Identified thermal fronts with a temperature distribution at 25 m depth from the AXBT surveys: Cheju-Yangtze Front (CYF), Cheju-Tsushima Front (CTF), Tsushima Front (TF), and Kuroshio Front (KF) (Park and Chu, 2007b).

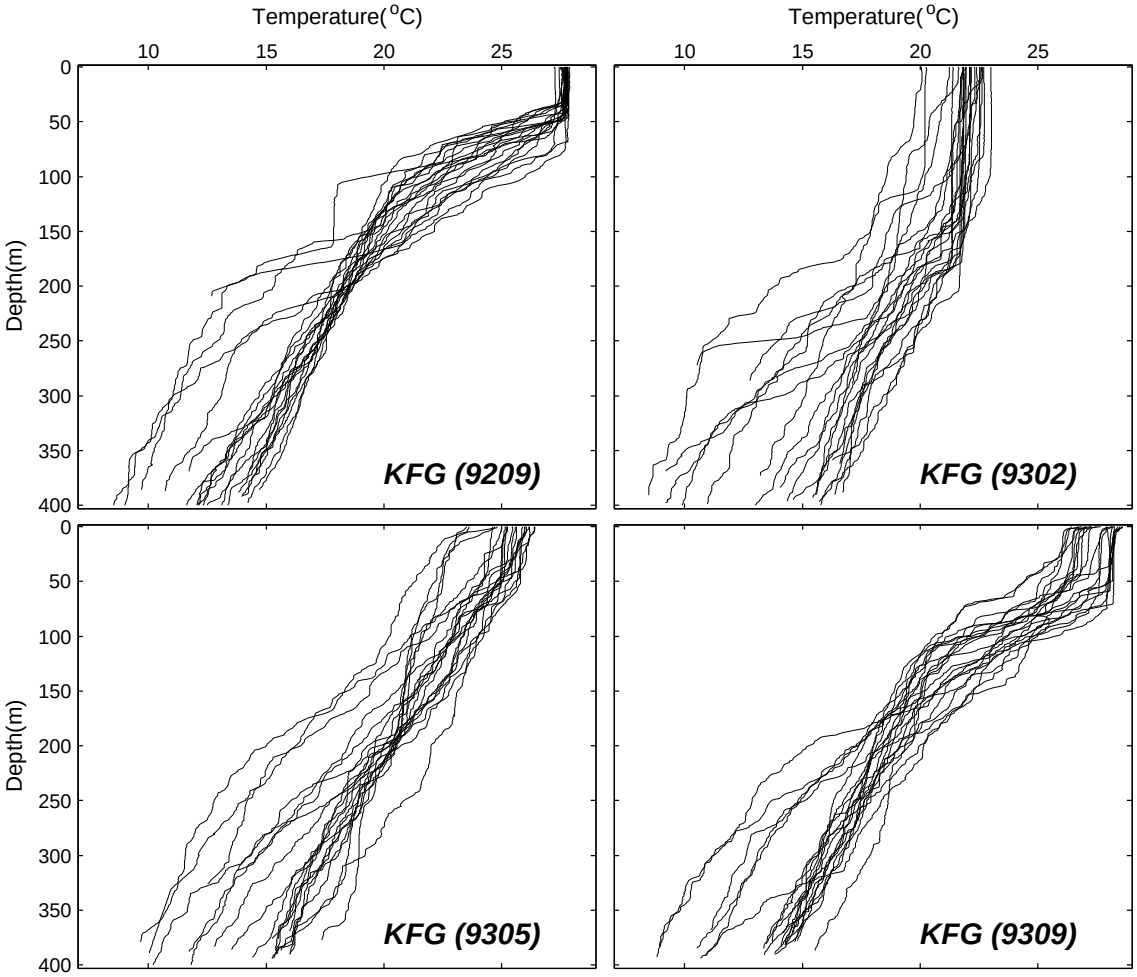

Figure 3. Temperature profiles in KFG (location see Fig. 2a)

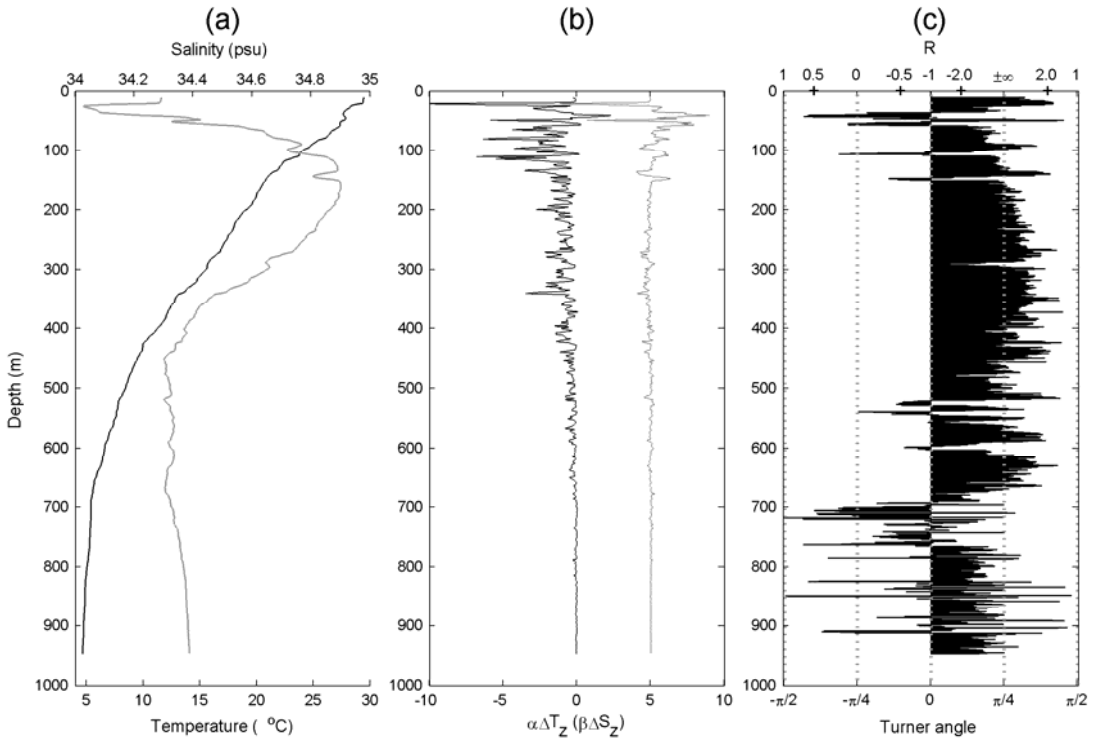

Figure 4. (a) Temperature (black curve) and salinity (grey curve) profiles observed at 127.14°E and 28.25°N in June 1994 (from WOD05), (b) vertical temperature gradient multiplied by the thermal expansion coefficient (α) (black curve) and haline gradient multiplied by the salinity contraction coefficient (grey curve) (unit: 10^{-5} m^{-1}), and (c) Turner angle and corresponding density ratio *R* (unit marked at the top).

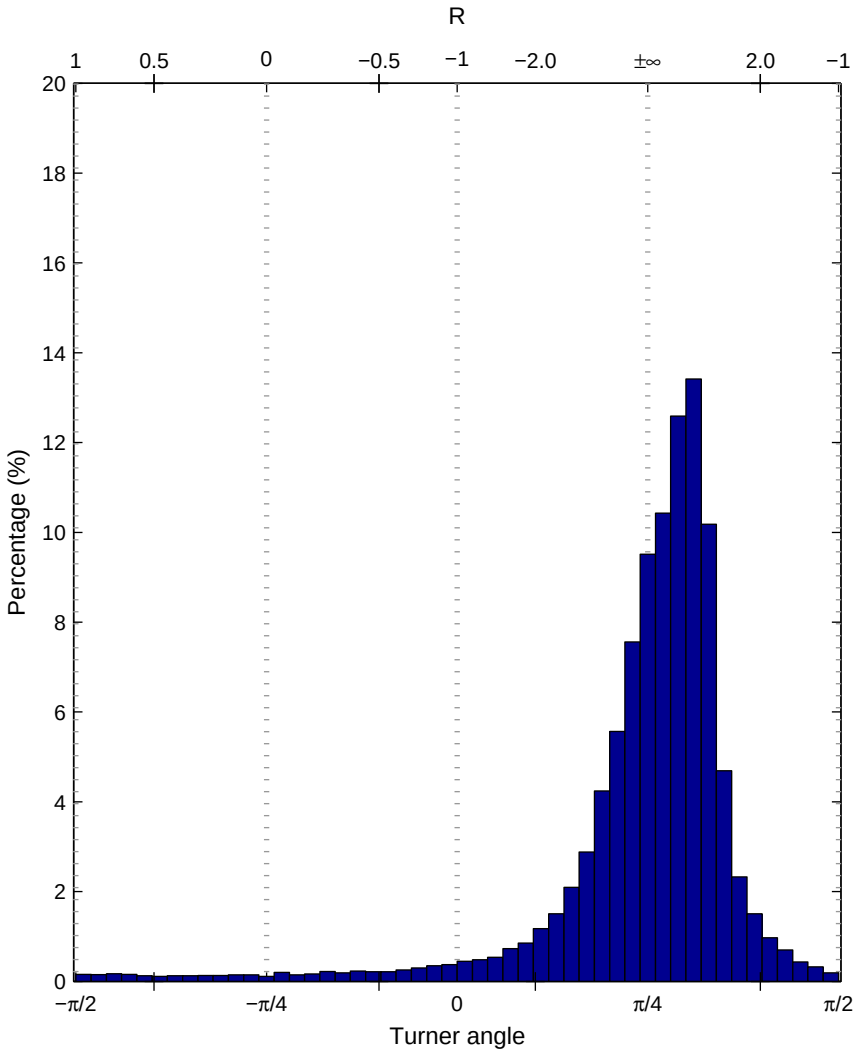

Figure 5. Histogram of the Turner angle (or density ratio R) calculated from 260 profiles (51−400 m) in the KFG with a bin size of π/50. The data are extracted from WOD05 for the period of 1991−2002. The density ratio *R* is marked at the top.

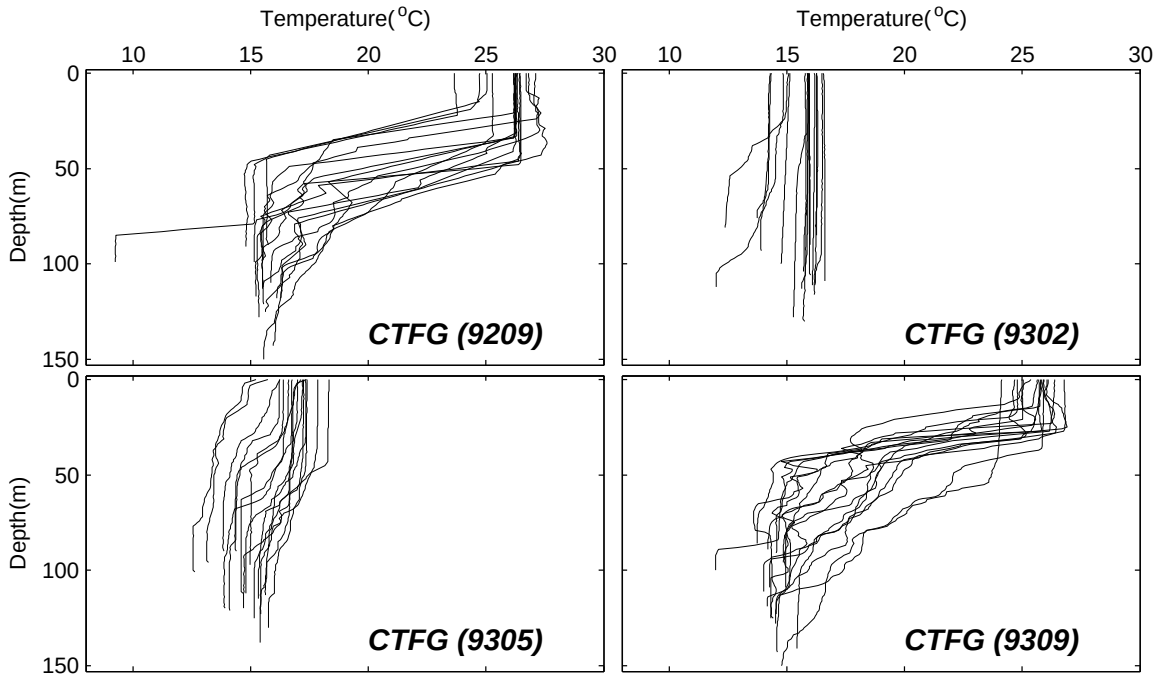

Figure 6. Temperature profiles in the CTFG (location see Fig. 2a).

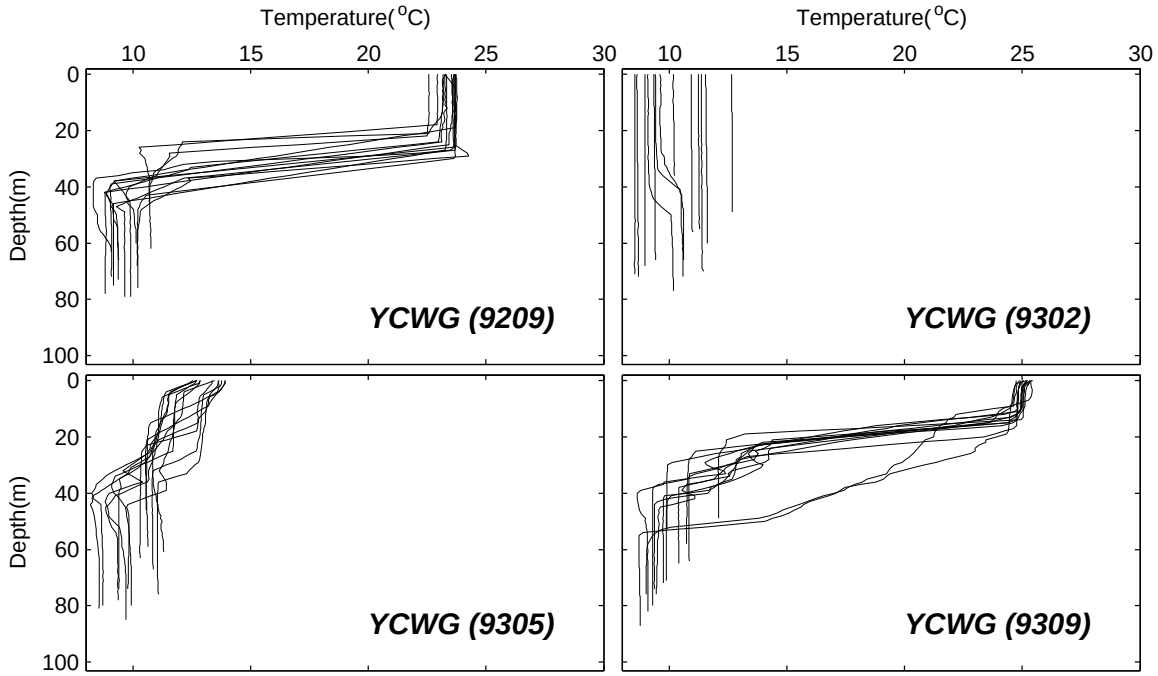

Figure 7. Temperature profiles in the YCWG (location see Fig. 2a).

1

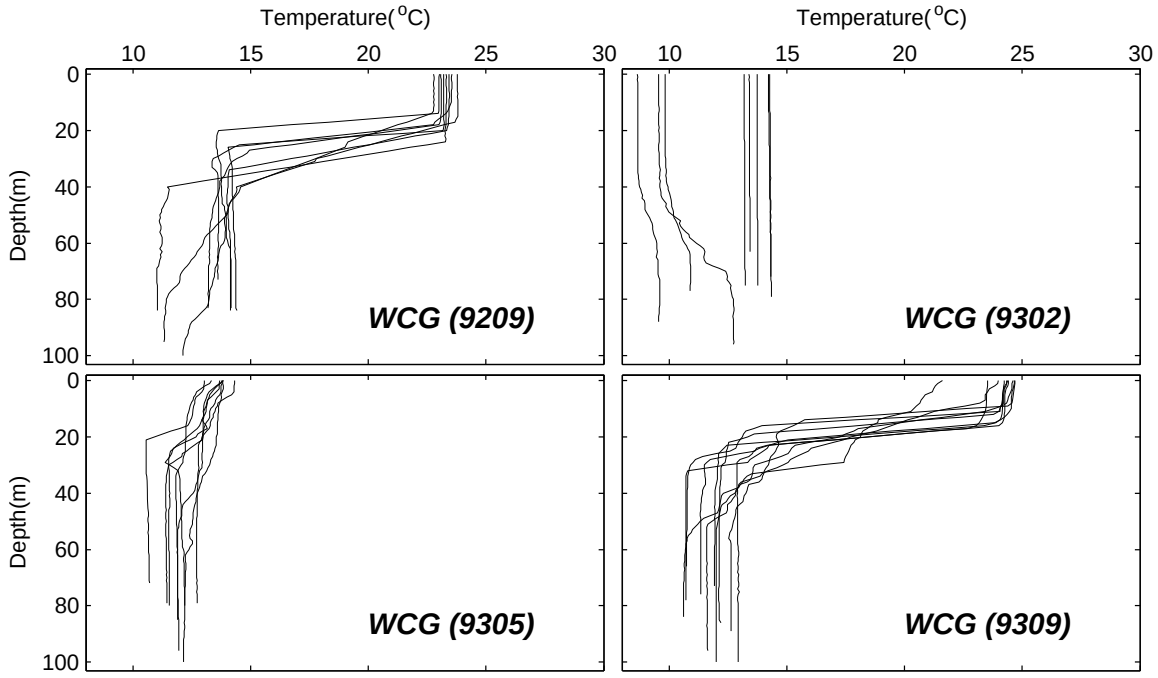

2

3 Figure 8. Temperature profiles in WCG (location see Fig. 2a).

4

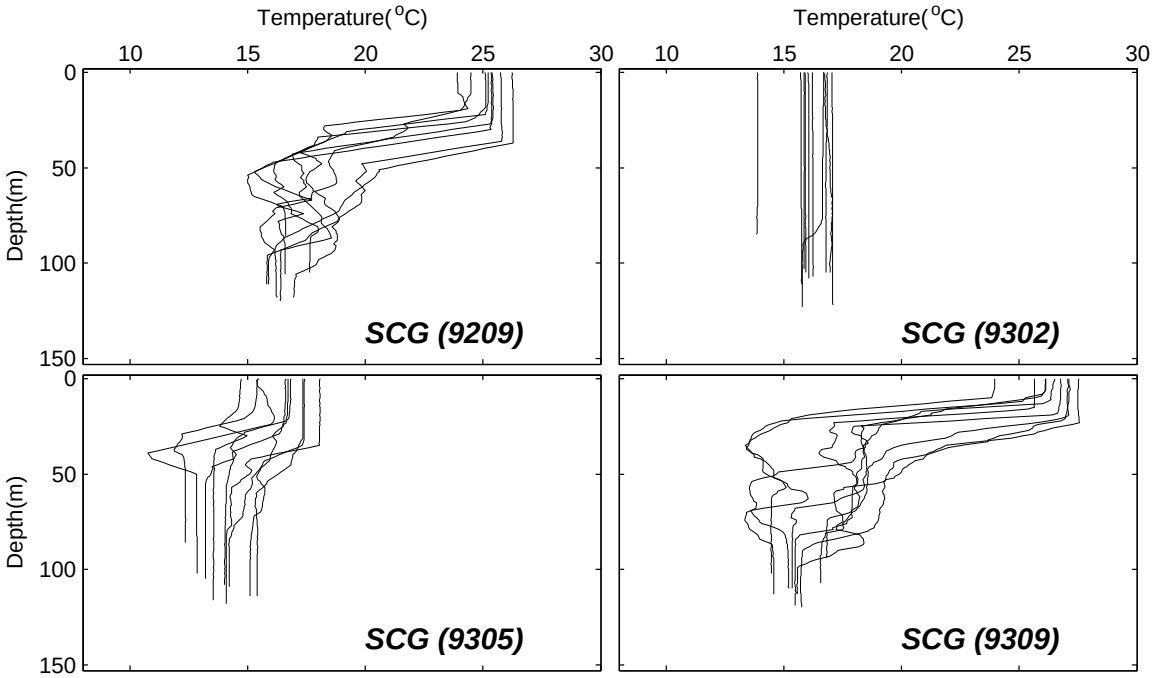

Figure 9. Temperature profiles in SCG (location see Fig. 2a).

1

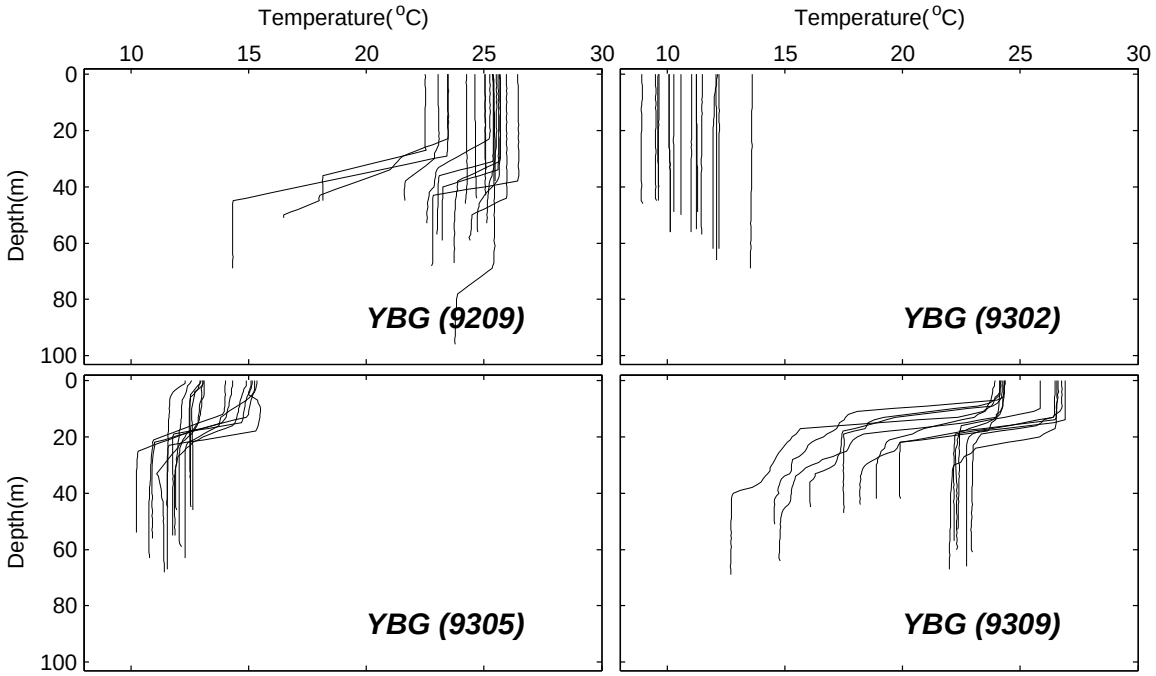

2

3 Figure 10. Temperature profiles in YBG (location see Fig. 2a).

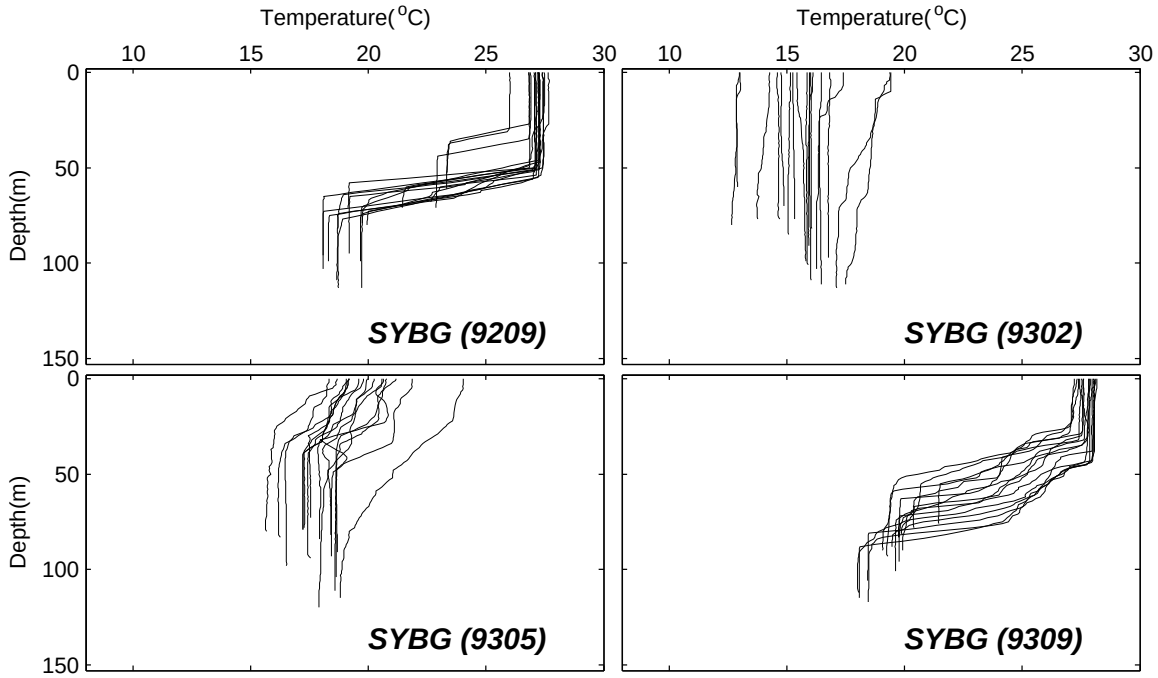

Figure 11. Temperature profiles in SYBG (location see Fig. 2a).

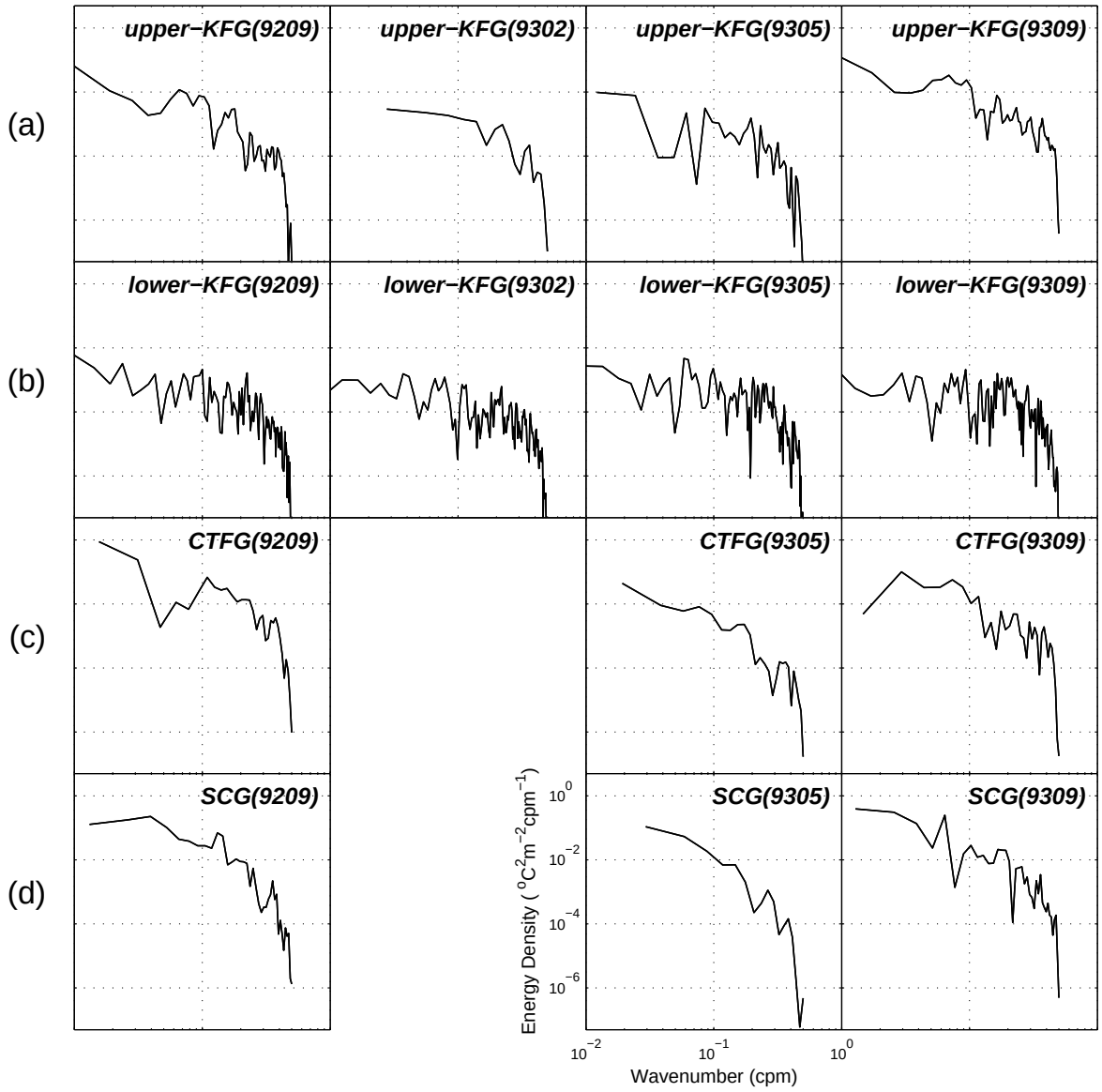

Figure 12. Spectra of vertical temperature gradient in various groups with KFG divided into upper segment (upper-KFG, shallower than 150 m) and lower segment (lower-KFG, 151−400 m).

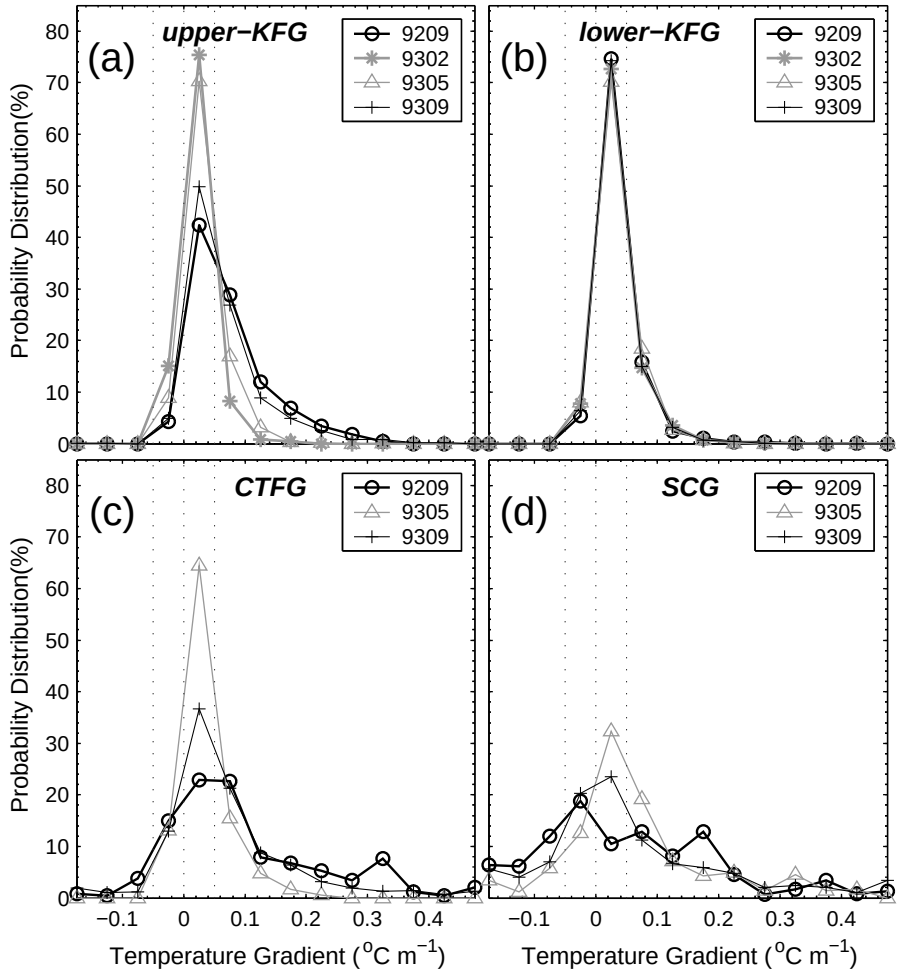

Figure 13. Ensemble-averaged PDFs of vertical temperature gradient with bin size of 0.05 °C m^{-1} for: (a) upper-KFG, (b) lower-KFG, (c) CTFG, and (d) SCG.

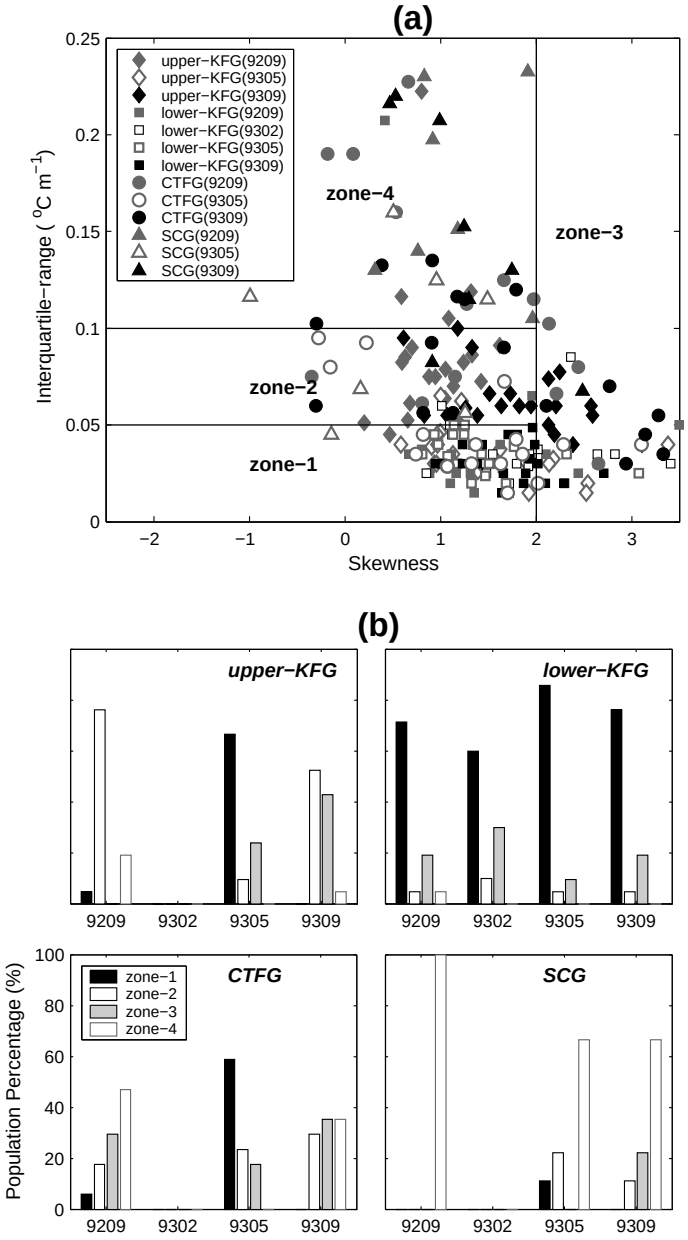

Figure 14. (a) Scatter diagram of interquartile-range vs. skewness of vertical temperature gradient for the same groups in Fig. 10 (see details in the text) with four zones: zone-1 (interquartile-range ≤ 0.05 and skewness ≤ 2), zone-2 ($0.05 <$ interquartile-range ≤ 0.1 and skewness ≤ 2), zone-3 (skewness > 2), and zone-4 (interquartile-range > 0.1 and skewness ≤ 2). (b) Histograms of occurrence percentage of the four zones.

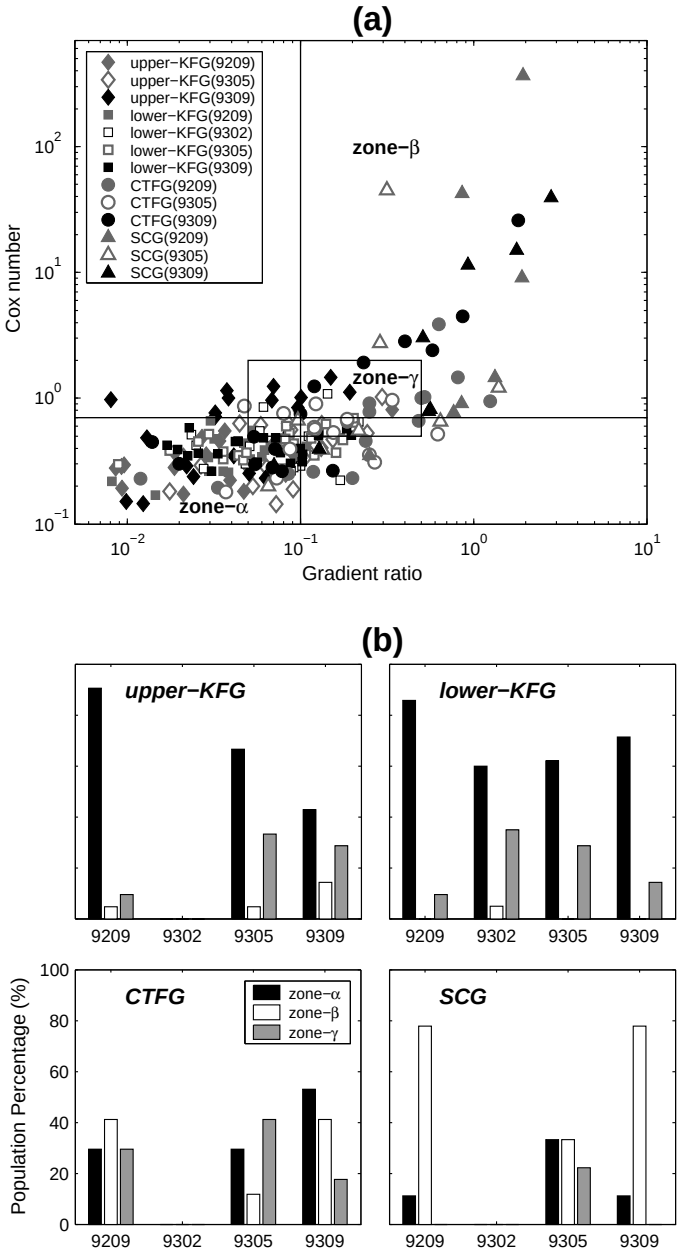

Figure 15. (a) Scatter diagram of Cox number vs. gradient ratio of vertical temperature gradient for the same groups as in Fig. 10 (see details in the text) with three zones: zone-α (Cox number ≤ 0.7 and gradient ratio ≤ 0.1), zone-β (Cox number > 0.7 and gradient ratio > 0.1), and zone-γ ($0.5 <$ Cox number ≤ 2 and $0.05 <$ gradient ratio ≤ 0.5). (b) Histograms of occurrence percentage of the three zones.

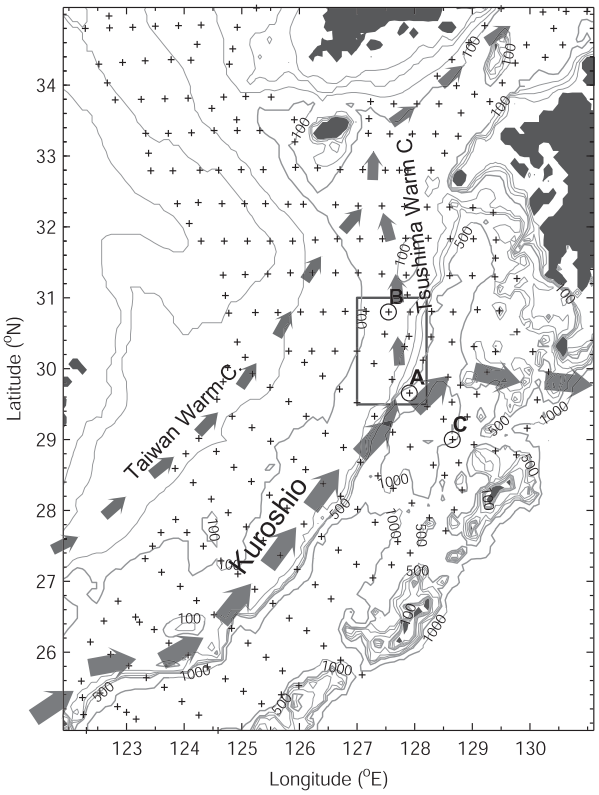

Figure 16. Systematic of the current system in the East China Sea. The Kuroshio following along the continental shelf is separated into the northern branch, i.e. the Tsushima Warm Current, and the eastern northern branch at 127–127°E and 29–30°N, which is assumed as the Tsushima Warm Current branching location (Huh, 1982; Lie *et al.*, 1998; Hsueh, 2000; Furey and Bower, 2005). The Taiwan Warm Current, which passes through the Taiwan Strait and then flows over the continental shelf, contributes to the Tsushima Warm Current in warm seasons (Isobe, 1999; Ichikawa and Beardsley, 2002). The AXBT stations are marked by a cross. Three individual AXBT profiles marked by an open circle are used for calculating spectral and statistical values in the Tsushima Warm Current branching region: a station at the branching location labeled by "A" and the two neighboring stations labeled by "B" and "C" (Stn-A, Stn-B, and Stn-C, respectively). A box is for Fig. 17.

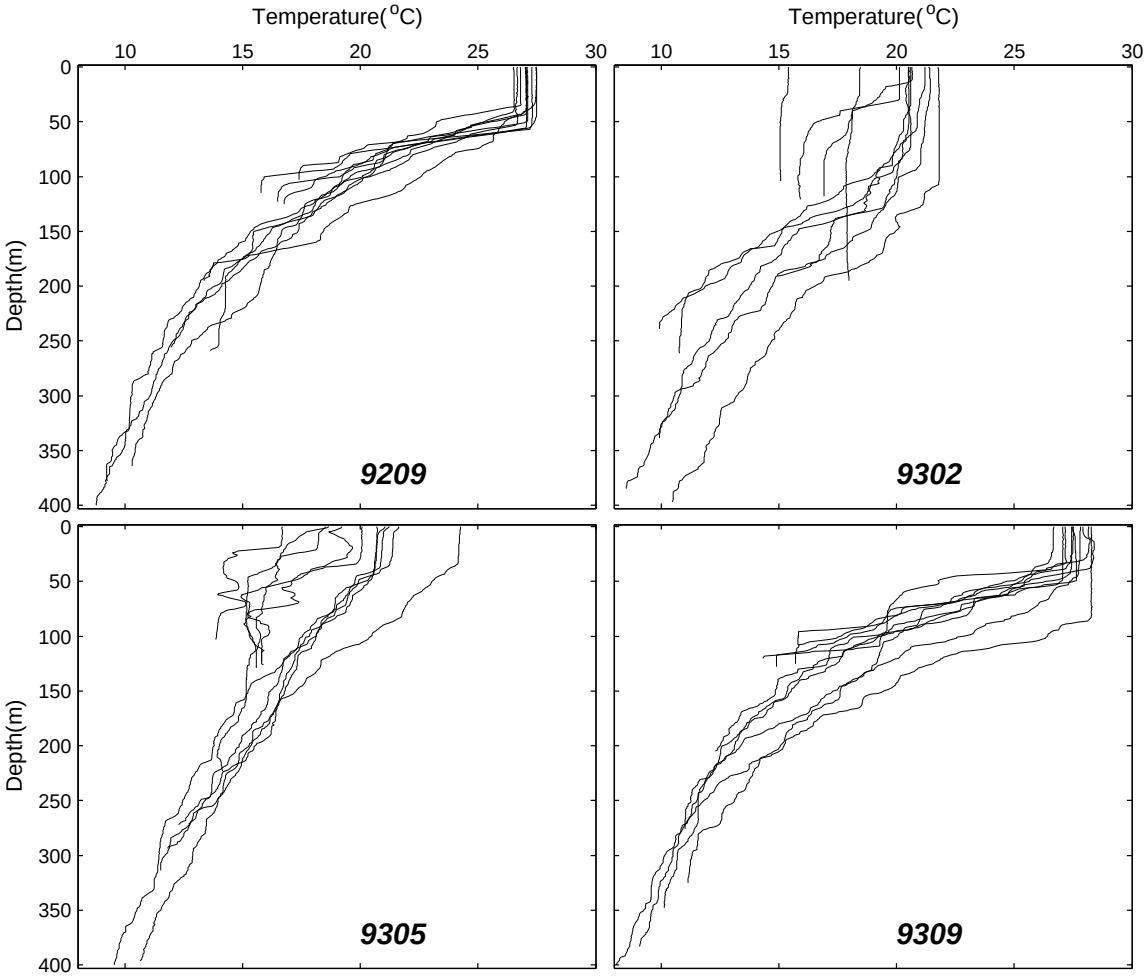

Figure 17. Temperature profiles in the Tsushima Warm Current branching region (inside the box indicated in Fig. 16).

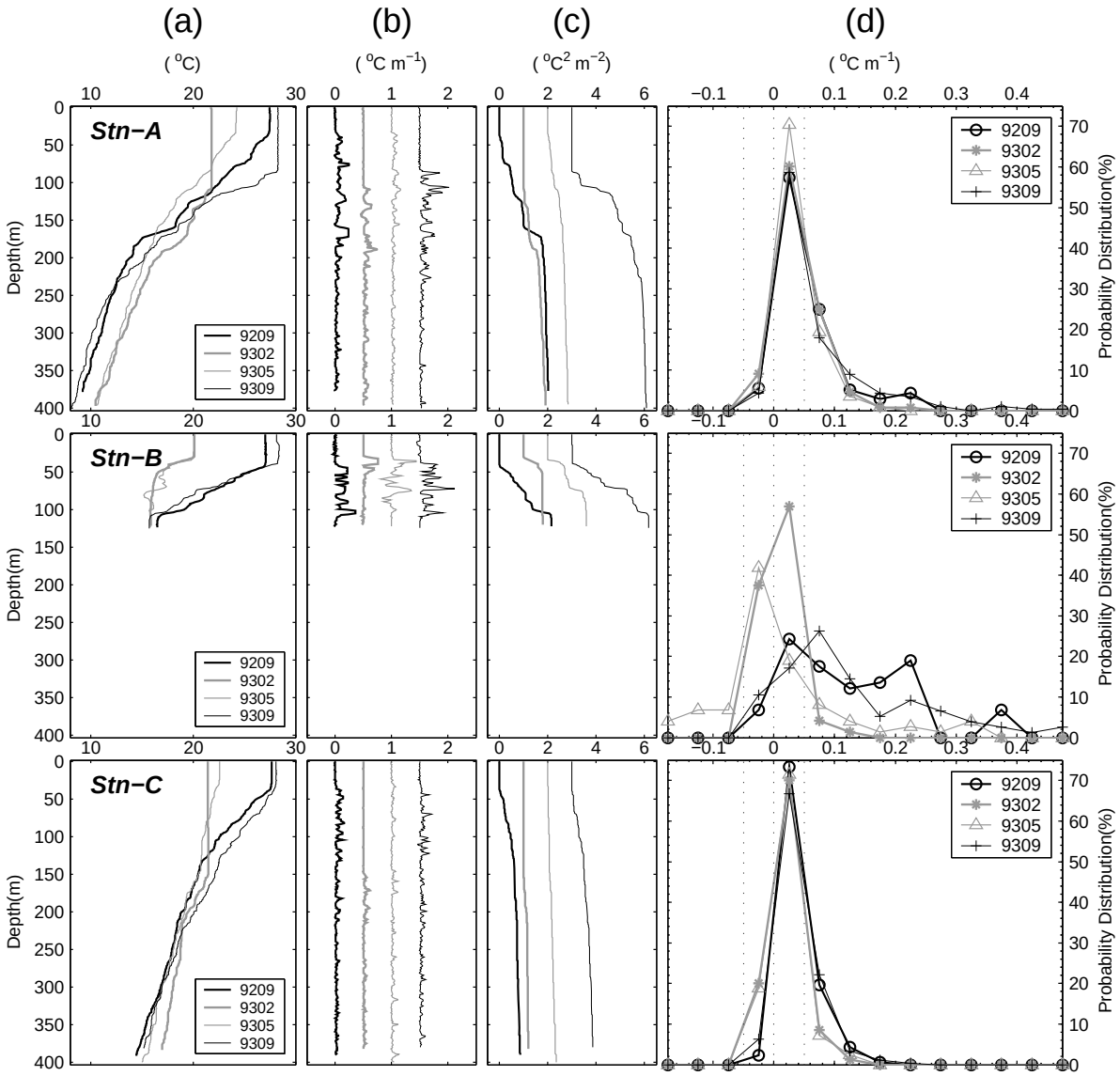

Figure 18. (a) Temperature profiles, (b) vertical temperature gradient, (c) cumulative variance of vertical temperature gradient, and (d) probability distribution function of vertical temperature gradient for three stations in the Tsushima Warm Current branching region (location see Fig. 16) with the first row for Stn-A, second row for Stn-B, and third row for Stn-C. In (b) and (c) the profile 9209 is in correct scale shown at the top and remaining profiles are offset by 0.5 ºC m^{-1} and 1 ºC^2 m^{-2}, respectively.

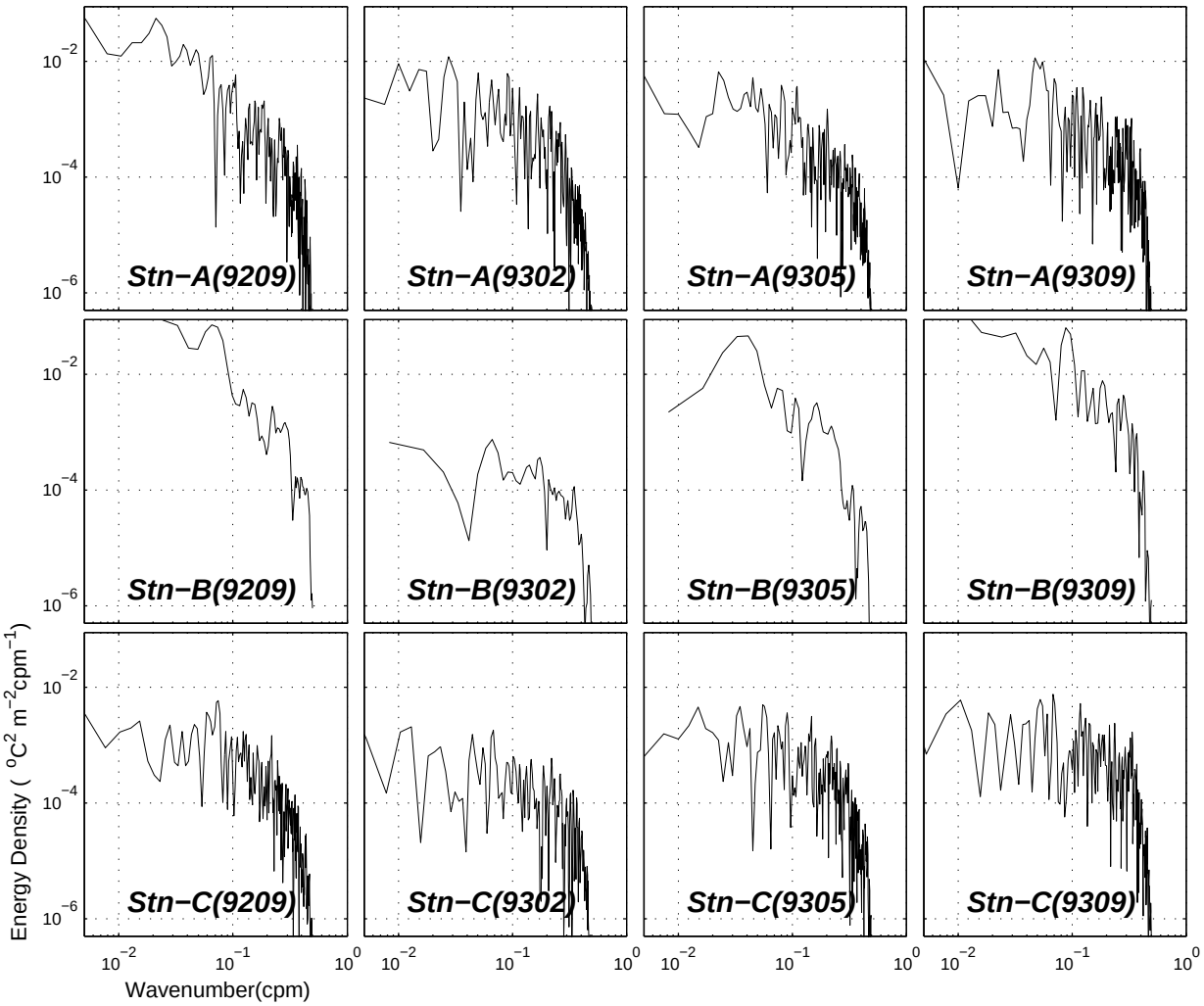

Figure 19. Spectra of vertical temperature gradient of the three stations in the Tsushima Warm Current branching region (location see Fig. 16).